CELL BIOLOGY

Excessive exosome release is the pathogenic pathway linking a lysosomal deficiency to generalized fibrosis

Diantha van de Vlekkert[1], Jeroen Demmers[2], Xinh-Xinh Nguyen[3], Yvan Campos[1], Eda Machado[1], Ida Annunziata[1], Huimin Hu[1], Elida Gomero[1], Xiaohui Qiu[1], Antonella Bongiovanni[4], Carol A. Feghali-Bostwick[3], Alessandra d'Azzo[1,5]*

Lysosomal exocytosis is a ubiquitous process negatively regulated by neuraminidase 1 (NEU1), a sialidase mutated in the glycoprotein storage disease sialidosis. In *Neu1*$^{-/-}$ mice, excessive lysosomal exocytosis is at the basis of disease pathogenesis. Yet, the tissue-specific molecular consequences of this deregulated pathway are still unfolding. We now report that in muscle connective tissue, *Neu1*$^{-/-}$ fibroblasts have features of myofibroblasts and are proliferative, migratory, and exocytose large amounts of exosomes. These nanocarriers loaded with activated transforming growth factor–β and wingless-related integration site (WNT)/β-catenin signaling molecules propagate fibrotic signals to other cells, maintaining the tissue in a prolonged transitional status. Myofibroblast-derived exosomes fed to normal fibroblasts convert them into myofibroblasts, changing the recipient cells' proliferative and migratory properties. These findings reveal an unexpected exosome-mediated signaling pathway downstream of NEU1 deficiency that propagates a fibrotic disease and could be implicated in idiopathic forms of fibrosis in humans.

INTRODUCTION

Mammalian tissues and organs preserve their structural and functional homeostasis by means of their supportive connective tissue, a three-dimensional network of cells and extracellular matrix (ECM) with different topological characteristics depending on the organ/tissue in which it is embedded (*1*). Connective tissue resident fibroblasts are the primary cells that produce and secrete the interstitial ECM, which defines the extent of tissue stiffness and architecture (*1*, *2*). Deposition and remodeling of the ECM occur physiologically during development and organ differentiation and, in the adult, during tissue regeneration or repair and wound healing following injury and inflammation (*1*). In the case of chronic forms of tissue damage, increased production and deposition of the ECM result in a fibrotic disease that ultimately leads to organ failure (*1*, *3*). Activated fibroblasts or myofibroblasts are primarily responsible for the development and amplification of the fibrotic process (*3*, *4*). Myofibroblasts acquire a spindle-shape or stellate morphology, are contractile and motile, express α–smooth muscle actin (αSMA), and secrete excess amounts of ECM components (*3*, *4*). These cells mostly originate from resident, quiescent, or resting fibroblasts in response to specific cues from the local microenvironment (*3*, *4*), but they may also derive from other precursor cells, including resident mesenchymal progenitor cells, muscle satellite cells, and the recently found fibro/adipogenic progenitors (FAPs) (*5*).

Canonical effectors of fibrosis are the transforming growth factor–β (TGF-β) and wingless-related integration site (WNT) families of secreted ligands (*6*). TGF-β is the prototypical profibrotic cytokine, which can, by itself, stimulate the synthesis of ECM components by myofibroblasts and up-regulate the transcription of TGF-β target genes via nuclear accumulation of phosphorylated SMAD2/3 (pSMAD2/3) in complex with SMAD4 (*6*). The newly synthesized TGF-β precursor undergoes dimerization, glycosylation, and proteolytic cleavage, giving rise to a dimeric form that comprises the inactive mature cytokine bound to the latency-associated peptide (LAP) (*6*). En route to the extracellular space, this small TGF-β1 complex associate with the latent TGF-β–binding protein, which is then secreted and further processed extracellularly, releasing the active cytokine (*6*). WNTs are a class of 19 secreted, lipid-modified glycoproteins that mediate several intracellular signaling processes, acting as ligands for target membrane receptors and binding to other secreted proteins or proteoglycans (*7*). Intracellular WNT signaling is generally categorized into canonical, which signals through β-catenin, and noncanonical, which is β-catenin independent (*8*). In the canonical pathway, WNT binding to Frizzled (FZD) and its co-receptor low-density lipoprotein receptor-related protein 5/6 (LRP5/6) triggers the stabilization and nuclear translocation of cytosolic β-catenin, which, in association with T cell factor/lymphoid enhancer-binding factor (TCF/LEF), induces the transcription of genes involved in proliferation and apoptosis (*9*). Noncanonical WNT signaling comprises the WNT/Ca^{2+} and WNT/planar cell polarity pathways that regulate cell polarity, cell movement, and cytoskeletal rearrangement, through WNT binding to FZD and the co-receptors, ROR1, ROR2, and RYK (*8*, *9*). Both TGF-β and WNT signaling pathways, independently or cooperatively, can foster changes in the cells' gene expression profile and up-regulate basic epithelial-to-mesenchymal transition (EMT)–inducing transcription factors, including *Snai1*, *Snai2*, *Zeb1*, *Zeb2*, *Twist*, and *TCF/Lef1* (*10*). The ensuing loss of cell-cell contact and cell polarity, coupled to reorganization of the cytoskeletal network, allows cells to attain stem cell–like features, to secrete excessive ECM components (i.e., collagens and fibronectin), and to become motile, invasive, and resistant to apoptosis and senescence (*10*).

Remodeling/degradation of the ECM is controlled by the balanced processes of ECM proteins' deposition and degradation during wound healing or tissue repair (*11*). A key role in ECM remodeling is played by exosomes, dynamic nanovesicles that are secreted by virtually all

[1]Department of Genetics, St. Jude Children's Research Hospital, 262 Danny Thomas Place, Memphis, TN 38105, USA. [2]Proteomics Center, Erasmus University Medical Center, Wytemaweg 80, 3015 CN, Rotterdam, Netherlands. [3]Division of Rheumatology and Immunology, Department of Medicine, Medical University of South Carolina, Charleston, SC 29425, USA. [4]Institute of Biomedicine and Molecular Immunology (IBIM), National Research Council (CNR) of Italy, Palermo, Italy. [5]Department of Anatomy and Neurobiology, The University of Tennessee Health Science Center, Memphis, TN 38163, USA.
*Corresponding author. Email: sandra.dazzo@stjude.org

cells and are found in all biological fluids (*12*). With their heterogeneous contents, exosomes have emerged as central mediators of cell-cell communication; they can serve as delivery carriers for the exchange between cells of soluble proteins, microRNAs, and mRNAs but can also initiate signaling pathways in the receiving cells, thereby changing their biological properties (*12*). Thus, exosomes can act as a double-edged sword, being important modulators of normal tissue physiology and are also able to trigger and propagate pathological stimuli (*12*).

Processing/degradation of the ECM requires the action not only of matrix metalloproteinases (MMPs) but also of lysosomal cathepsins (*11*). The discharge of active lysosomal enzymes extracellularly occurs via lysosomal exocytosis, which is negatively regulated by the lysosomal sialidase neuraminidase 1 (NEU1) (*13*, *14*). During this calcium-dependent process, a pool of lysosomes are recruited along the cytoskeleton for transport to and docking at the plasma membrane (PM), before their fusion with the PM and the release of their contents (*13*, *14*). In NEU1-deficient cells, an increased number of lysosomes dock at and fuse with the PM, which results in excessive lysosomal exocytosis (*14*). This altered process is the basis of pathogenesis in the *Neu1*$^{-/-}$ mouse (*14*–*18*), a faithful model of the lysosomal glycoprotein storage disease sialidosis (*19*, *20*). Patients with sialidosis present with a spectrum of disease severity and are usually classified on the basis of the age of onset of their symptoms as type I, the mild form with onset in the second decade of life and longer survival, or type II, the severe, early-onset form associated with poor prognosis (*19*, *21*). As patients with this disease, *Neu1*$^{-/-}$ mice develop severe muscle atrophy, which is linked to relentless expansion of the muscle connective tissue, associated with increased cellularity, massive deposition of ECM, and activation of MMPs, in the absence of an overt inflammatory response (*18*). Expanded connective tissue ultimately invades the muscle bed, leading to muscle fiber fragmentation and degeneration (*18*). Although the pathologic sequel of this myopathy is obvious, the question remains as to how NEU1 deficiency provokes the connective tissue disease and which are the molecular effectors.

Here, we address this question mechanistically by investigating the role of exosomes exocytosed by *Neu1*$^{-/-}$ muscle connective tissue fibroblasts in the fibrotic process. We found that *Neu1*$^{-/-}$ fibroblasts are activated into myofibroblasts by a self-perpetuating mechanism driven by exosomes that keep these cells in a constant status of transdifferentiation reminiscent of tumor cells. Exosomes exocytosed in excess by NEU1-deficient cells and loaded with profibrotic signaling molecules are capable of inducing fibrotic features in normal fibroblasts. This exosome-mediated pathogenic pathway downstream of NEU1 deficiency has never been described in a pediatric lysosomal storage disease. On the basis of our findings, deregulated levels of this enzyme should be sought as a contributing factor in some of the numerous idiopathic forms of fibrosis in humans.

RESULTS

Neu1$^{-/-}$ fibroblasts have features of myofibroblasts

In the *Neu1*$^{-/-}$ skeletal muscle, hypertrophy of the connective tissue and increased number of cells are aspects of advanced fibrosis, as evidenced by the massive deposition of collagen detected by Masson's trichrome staining of muscle sections (Fig. 1A). To identify the molecular pathway(s) underlying the hypertrophic connective tissue, we first examined the cell population(s) responsible for the increased cellularity. Fluorescence-activated cell sorting (FACS) analysis of cells isolated from adult skeletal muscle was performed using αSMA, a smooth muscle marker whose expression is induced in myofibroblasts, and T cell–specific transcription factor 4 (TCF4/TCF7L2), a marker of muscle connective tissue fibroblasts expressed during development and regeneration (*22*). This analysis showed that 80 to 95% of the cells were TCF4^{+} (1B) and there was a significantly higher percentage of TCF4/αSMA double-positive cells in the *Neu1*$^{-/-}$ muscle compared to wild type (WT; Fig. 1C). In both samples, we identified only a very small percentage of myogenic progenitors (MPs) and FAPs (Fig. 1, D and E). Note that the *Neu1*$^{-/-}$ connective tissue from 4.5-month-old mice contained a significantly lower number of MPs compared to WT (Fig. 1D), a finding that conformed with the delayed muscle regeneration seen in *Neu1*$^{-/-}$ mice (*18*). We further demonstrated that *Neu1*$^{-/-}$ myofibroblasts were significantly more proliferative than WT cells (Fig. 1F), albeit they retained the ability to migrate/invade both a synthetic ECM substrate (Matrigel) and peritoneal membranes derived from WT and *Neu1*$^{-/-}$ mice (Fig. 1, G to J). The fact that *Neu1*$^{-/-}$ myofibroblasts invaded the WT peritoneum more proficiently than WT cells demonstrated their cell-autonomous ability to migrate through a basement membrane. However, the *Neu1*$^{-/-}$ peritoneum was more receptive to invasion by either cell types than the WT peritoneum (Fig. 1J), denoting that remodeling/degradation of the ECM already occurred in the *Neu1*$^{-/-}$ peritoneum, rendering it more susceptible to invasion. Thus, loss of Neu1 induces changes in the makeup of *Neu1*$^{-/-}$ muscle connective tissue fibroblasts that promote their activation and transdifferentiation into myofibroblasts, which represent the predominant cell population that drives the fibrotic process.

Neu1$^{-/-}$ skeletal muscle fibrosis is driven by TGF-β signaling and is corrected by adeno-associated virus–mediated gene therapy

Given the ability of myofibroblasts to secrete profibrotic cytokines, we first assessed whether components of the TGF-β signaling pathway were deregulated in *Neu1*$^{-/-}$ muscle connective tissue. We found that the levels of TGF-β protein and its downstream target Smad2 and activated pSmad2 were markedly increased in the affected connective tissue (Fig. 2, A to D, and fig. S1, A to C). Furthermore, other canonical fibrotic markers, i.e., E-cadherin, vimentin, collagens I and IV, β-catenin, αSMA, and TCF4, were also significantly higher in the *Neu1*$^{-/-}$ connective tissue compared to WT (Fig. 2, E and F, and fig. S1, D to M). We also showed that cells expressing TCF4 in the affected areas were also positive for TGF-β1 (Fig. 2G). Particularly relevant was the observation that proteins such as periostin and osteopontin, both known to play a role in tissue regeneration/repair, inflammation, muscle dystrophies, and fibrosis (*23*, *24*), were exclusively detected in the affected connective tissue (fig. S2, A to E). We confirmed these results in cultured *Neu1*$^{-/-}$ myofibroblasts (Fig. 2, H and I, and fig. S3, A to L), indicating that these cells are the primary source of the profibrotic signals responsible for the induction and progression of the fibrotic disease leading to muscle atrophy.

The unusual myopathy in the *Neu1*$^{-/-}$ mice could be largely corrected by a single intravenous injection of two recombinant scAAV2/8 (self-complementary adeno-associated virus 2/8) vectors expressing human *NEU1* (fig. S3M) and its chaperone protective protein/cathepsin A (PPCA) (fig. S3M). Real-time quantitative polymerase chain reaction (RT-qPCR) of several fibrotic markers including *Tgfb* (Fig. 2J) and Masson's trichrome staining of muscle sections (Fig. 2K)

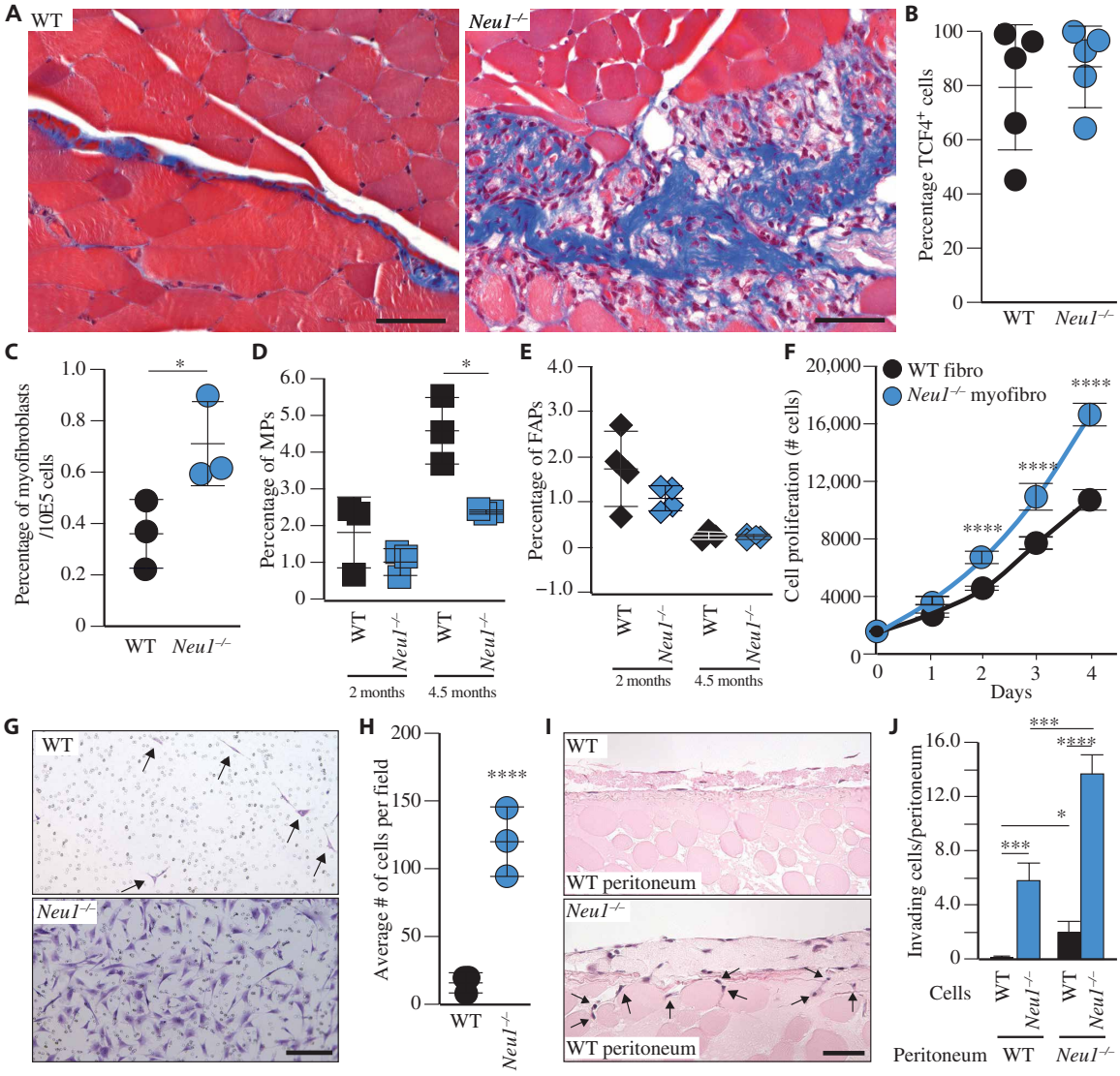

Fig. 1. *Neu1*$^{-/-}$ fibroblasts have characteristics of myofibroblasts. (**A**) Coronal gastrocnemius muscle sections of WT and *Neu1*$^{-/-}$ mice were stained with Masson's trichrome, demonstrating massive collagen deposition (blue) in the *Neu1*$^{-/-}$ muscle. Scale bars, 50 μm. (**B** and **C**) FACS analysis of muscle connective tissue fibroblasts (CD45$^-$/CD31$^-$/αSMA$^-$/TCF4$^+$, $n = 5$) (B) and myofibroblasts (CD45$^-$/CD31$^-$/αSMA$^+$/TCF4$^+$, $n = 3$) (C) isolated from WT and *Neu1*$^{-/-}$ skeletal muscle at 3 to 4 months of age. (**D** and **E**) FACS analysis of MPs (CD45$^-$/CD31$^-$/Sca1$^-$/integrin-α7$^+$, $n = 3$) (D), and FAPs (CD45$^-$/CD31$^-$/Sca1$^+$/integrin-α7$^-$, $n = 4$) (E) isolated from WT and *Neu1*$^{-/-}$ skeletal muscle at 2 and 4.5 months of age. (**F**) Cell proliferation assayed in WT and *Neu1*$^{-/-}$ (myo)fibroblasts ($n = 6$). (**G**) Representative images of the invasion/migration assays performed with WT and *Neu1*$^{-/-}$ (myo)fibroblasts. Scale bar, 200 μm. (**H**) Quantification of (G) ($n = 3$). (**I**) Representative images of ex vivo invasion/migration of WT and *Neu1*$^{-/-}$ (myo)fibroblasts using ex vivo cultured peritoneal membranes. Scale bar, 100 μm. (**J**) Quantification of (I) ($n = 4$). Values are expressed as means ± SD. Statistical analysis was performed using the Student *t* test; *$P < 0.05$, ***$P < 0.001$, ****$P < 0.0001$.

showed clear reversal of the muscle connective tissue phenotype, confirming NEU1 deficiency as the primary insult.

Neu1$^{-/-}$ myofibroblasts maintain a transitional, partially differentiated state

The capacity of *Neu1*$^{-/-}$ myofibroblasts to be simultaneously proliferative and migratory and their increased levels of profibrotic and ECM markers were indicative of their partial differentiation and transitional status. To prove this hypothesis, we probed an EMT PCR array, including profibrotic inducers and ECM genes, with total RNA from WT and *Neu1*$^{-/-}$ muscle tissues (fig. S4, A and B). The array's results confirmed the increased expression of many ECM components (i.e., collagens, fibronectin, vimentin, and osteopontin) and ECM-degrading enzymes and their inhibitors (i.e., MMPs and tissue inhibitor of MMPs) in the *Neu1*$^{-/-}$ muscle RNA. In addition, beside the up-regulation of TGF-β signaling molecules, we observed significant up-regulation of members of both the canonical and noncanonical WNT signaling pathways (fig. S4, A and B). RT-qPCR (Fig. 3, A to C) in total muscle RNA from WT and *Neu1*$^{-/-}$ mice of different ages (1 to 5 months) validated the results of the arrays. We found that members of the TGF-β superfamily (*Tgfb1*, *Tgfb2*, and *Tgfb3*), particularly *Tgfb1* and its target *Smad2*, increased progressively in *Neu1*$^{-/-}$ muscle, as the animals aged (Fig. 3A and fig. S4C). This was accompanied by the up-regulated expression of canonical

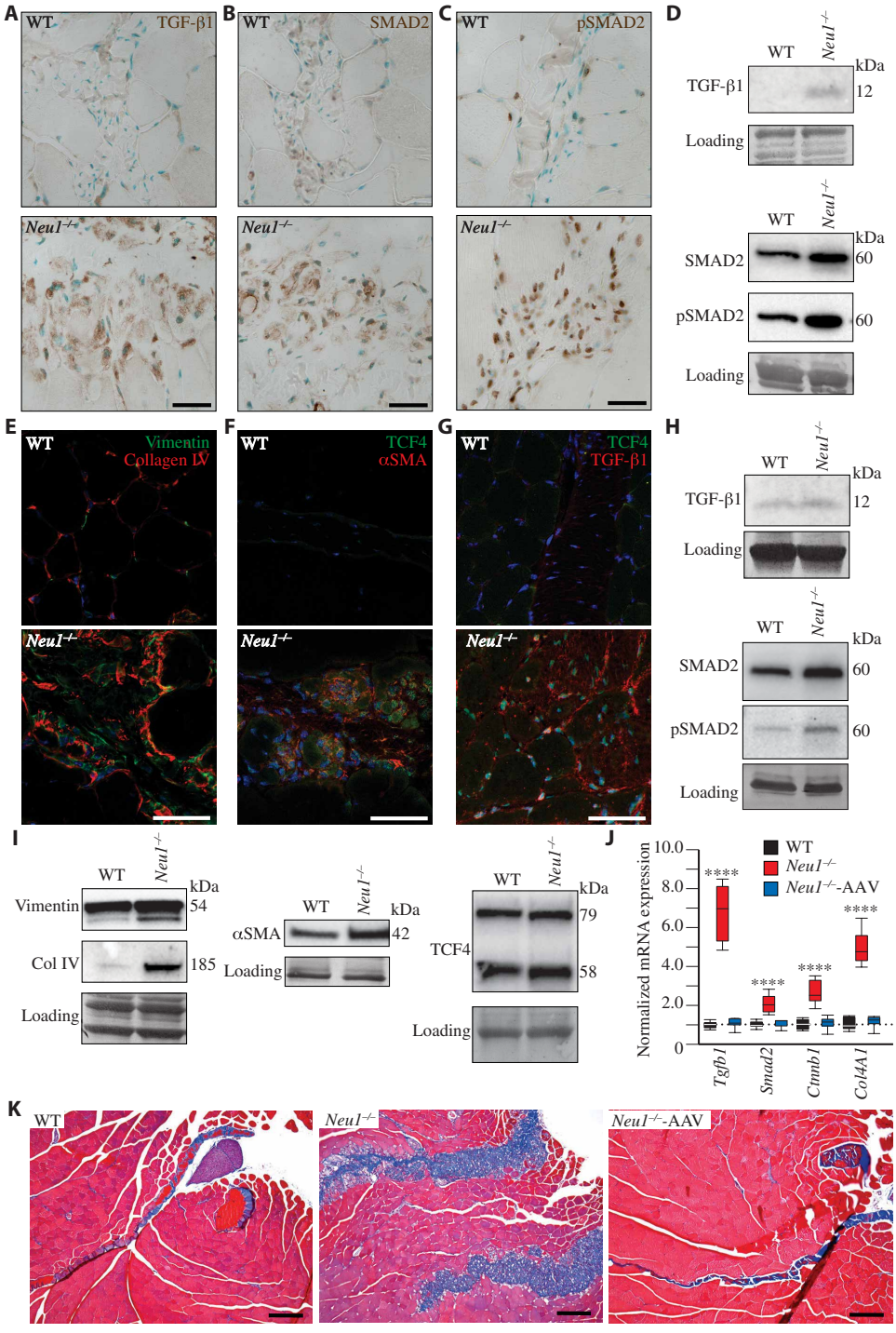

Fig. 2. TGF-β1 signaling drives fibrosis in *Neu1*$^{-/-}$ muscle, which is rescued by AAV-mediated gene therapy. (**A** to **C**) Immunohistochemical (IHC) analysis of WT and *Neu1*$^{-/-}$ gastrocnemius (GA) muscle sections performed with anti–TGF-β1 (A), anti-SMAD2 (B), and anti-pSMAD2 (C) antibodies. Scale bars, 25 μm. (**D**) Immunoblot analysis of WT and *Neu1*$^{-/-}$ total GA muscle lysates probed with anti–TGF-β1, anti-SMAD2, and anti-pSMAD2 antibodies. (**E** and **F**) Transverse sections of the WT and *Neu1*$^{-/-}$ muscles were costained with anti-vimentin (green) and anti–collagen IV (red) (E) and anti-TCF4/TCF7 (red) and anti-αSMA (green) (F) antibodies. (**G**) Transverse sections of the WT and *Neu1*$^{-/-}$ muscles were costained with anti-TCF4 (green) and anti-TGF-β1 (red) antibodies. (**H**) Immunoblot analysis of WT and *Neu1*$^{-/-}$ (myo)fibroblast lysates probed with anti–TGF-β1, anti-SMAD2, and anti-pSMAD2 antibodies. (**I**) Immunoblots of WT and *Neu1*$^{-/-}$ (myo)fibroblasts were probed with and anti-vimentin, anti–collagen IV, anti-αSMA, and anti-TCF4 antibodies. (**J**) RT-qPCR of the indicated mRNAs in WT, *Neu1*$^{-/-}$, and *Neu1*$^{-/-}$-AAV muscles ($n = 7$). mRNA levels are normalized by 18*S* ribosomal RNA (rRNA) and relative to WT control. (**K**) Coronal gastrocnemius skeletal muscle sections of WT, *Neu1*$^{-/-}$, and *Neu1*$^{-/-}$-AAV (scAAV2/8-CMV-huNEU and scAAV2/8-CMV-huPPCA) treated mice stained with Masson's trichrome, showing complete rescue of the muscle fibrosis. Scale bars, 200 μm. Values are expressed as means ± SD. Statistical analysis was performed using the Student *t* test; ****$P < 0.0001$.

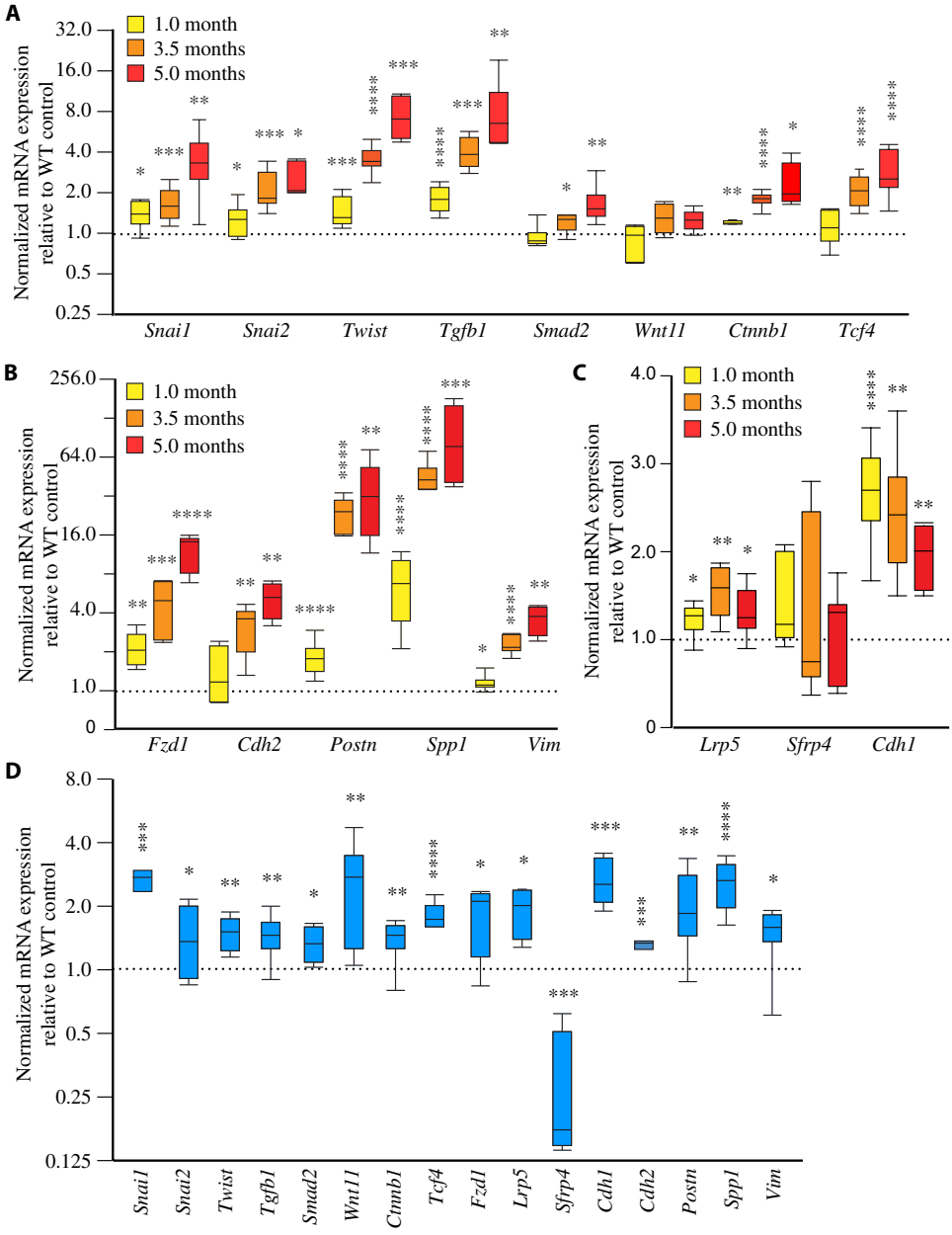

Fig. 3. *Neu1*$^{-/-}$ muscle and myofibroblasts up-regulate canonical markers of EMT. (**A** to **D**) RT-qPCR of the indicated mRNAs in *Neu1*$^{-/-}$ muscle from 1-, 3.5-, and 5-month-old mice ($n \geq 3$) (A to C) and in *Neu1*$^{-/-}$ myofibroblasts ($n \geq 3$) (D). Levels of normalized mRNA expression (by 18*S* rRNA) were relative to WT control. Values are expressed as means ± SD. Statistical analysis was performed using the Student *t* test; **P* < 0.05, ***P* < 0.01, ****P* < 0.001, *****P* < 0.0001.

EMT-inducing transcription factors, i.e., *Snai1*, *Snai2*, and *Twist* (Fig. 3A), suggesting a hybrid epithelial/mesenchymal status in the *Neu1*$^{-/-}$ muscle connective tissue, closely resembling the EMT/mesenchymal-to-epithelial transition (MET) process characteristic of highly aggressive sarcomas (*25*). Concomitantly, components of the WNT signaling pathway, i.e., β-catenin (*Ctnnb1*), glycogen synthase kinase 3β (*Gsk3b*), *Lrp5* and *Lrp6*, *Fzd1*, and calcium/calmodulin-dependent protein kinase II inhibitor 1 (*Camk2n1*) were significantly increased, while secreted frizzled-related protein 4 (*Sfrp4*), which inhibits the binding of WNTs to their receptors, was down-regulated (Fig. 3, A to C, and fig. S4C). Last, there was a time-dependent activation of mesenchymal markers, such as N-cadherin (*Cdh2*), periostin (*Postn*), osteopontin (*Spp1*), and vimentin (*Vim*), and a corresponding gradual down-regulation of E-cadherin (*Cdh1*) in the muscle of aging *Neu1*$^{-/-}$ mice (Fig. 3, B and C). As seen in muscle tissue, we also observed an altered mRNA expression of canonical EMT inducers in muscle-derived *Neu1*$^{-/-}$ myofibroblasts (Fig. 3D and fig. S4D). Collectively, these results suggest that in the *Neu1*$^{-/-}$ muscle connective tissue, WNT and TGF-β pathways cooperate in eliciting the fibrotic process that is driven and propagated by myofibroblasts, retaining a partially differentiated, transitional status.

Neu1$^{-/-}$ exosomes propagate profibrotic signals from cell to cell

We have reported earlier that the loss of NEU1 activity results in exacerbated lysosomal exocytosis of hydrolytic enzymes by various mouse cells, fibroblasts from patients with sialidosis, and human tumor cell lines (*14*–*16*, *18*). We therefore asked whether additional endolysosomal components were abnormally expelled by Neu1-deficient cells, focusing on exosomes. Purified exosomes from the medium of *Neu1*$^{-/-}$ myofibroblasts preserved the characteristic cup shape and size (fig. S5A), but their yield was about 20% higher than that of WT exosomes (fig. S5, B and C). To further validate their identity, we ran exosomes on sucrose density gradients and individual fractions analyzed on immunoblots probed with antibodies for selected exosomal markers, Alix, CD9, and CD81 (fig. S5D). The fractionation pattern of these markers showed that both *Neu1*$^{-/-}$ and WT exosomes sedimented in fractions 3 to 6 (1.10 to 1.14 g/ml) (*26*) of the gradients but marker levels were considerably higher in the *Neu1*$^{-/-}$ than in the WT samples (fig. S5D).

Comparative high-throughput proteomic analyses of *Neu1*$^{-/-}$ and WT exosomal fractions unequivocally demonstrated a robust increase in the *Neu1*$^{-/-}$ samples of proteins belonging to the TGF-β and both canonical and noncanonical WNT signaling pathways (table S2). Notwithstanding, *Neu1*$^{-/-}$ exosomes also contained high levels of glypicans (table S2), known to be required for efficient TGF-β1 signaling (*27*), and, for scaffolding and regulating, lipid-modified WNTs (*7*). The proteomic results were further validated by immunoblot analyses. Exosomal markers were increased in the *Neu1*$^{-/-}$ preparations, confirming the higher yield of exosomes purified from *Neu1*$^{-/-}$-conditioned medium compared to WT medium (Fig. 4A and fig. S5, E to K). Several members of the WNT pathways, including β-catenin, GSK3β and LRP5, and both WNT3a and WNT5a/b, were increased in amounts in *Neu1*$^{-/-}$ exosomes (Fig. 4B and fig. S6, A to E and H). Concomitantly, we detected high levels of the processed TGF-β1 monomer (~12 kDa) and dimer (~25 kDa) in exosomal lysates resolved on SDS gels under reducing and nonreducing conditions, respectively (Fig. 4C and fig. S6, F and H). The marked difference in the amount of TGF-β1 between *Neu1*$^{-/-}$ and WT exosomal preparations was even more obvious when blots were probed with a LAP-specific antibody that detected a 37.5-kDa protein under reducing conditions and a large complex of >250 kDa under nonreducing conditions (Fig. 4D and fig. S6, G and H). Unexpectedly, the pattern of expression of the TGF-β1 forms in *Neu1*$^{-/-}$ exosomes closely paralleled that identified in extracellular nanovesicles isolated from cancer cells (*28*).

To further probe into this parallel, we tested the localization of TGF-β1 in *Neu1*$^{-/-}$ and WT exosomal samples by subjecting the purified preparations to a mild proteinase K treatment, which removed the outer membrane proteins leaving the vesicles intact. We found that upon this treatment, both TGF-β1 monomer and its LAP were gradually stripped off the exosomes' outer membrane layer, while β-catenin, encased in the exosomal lumen, remained unaltered (Fig. 4E and fig. S6, I to M). We also demonstrated that WNT5a/b had a topological distribution similar to TGF-β1 because it was associated with the outer site of the exosomal membranes (Fig. 4E and fig. S6, I and M). These findings imply that NEU1 deficiency promotes excessive release of exosomes loaded with TGF-β and WNTs on their outer membranes. This topological configuration, so far only described in cancer cell–derived exosomes, should allow for the rapid propagation of fibrotic signals from cell to cell.

We tested this hypothesis using exosomes purified from the medium of WT fibroblasts or *Neu1*$^{-/-}$ myofibroblasts to condition the culture media of human and murine control cells. We found that *Neu1*$^{-/-}$ exosomes were able to induce a higher proliferation rate in murine and human control fibroblasts than WT exosomes (Fig. 5A and fig. S7A). Exosomes isolated from the culture medium of sialidosis-derived fibroblasts also induced increased proliferation rate of human and murine control fibroblasts (Fig. 5B and fig. S7B), suggesting that this exosome-mediated mechanism is pathognomonic of sialidosis in patients. We further demonstrated that WT fibroblasts cocultured with *Neu1*$^{-/-}$ exosomes had increased capacity to migrate through a synthetic ECM substrate compared to those cocultured with WT exosomes (Fig. 5C). Thus, *Neu1*$^{-/-}$ exosomes are efficient carriers of signaling molecules that control both proliferation and migration/invasion.

Neu1$^{-/-}$ exosomes convert normal fibroblasts into myofibroblasts

To further investigate the functional characteristics of *Neu1*$^{-/-}$ exosomes, we tested whether they could alter the gene expression profile of profibrotic markers (table S1) in murine and human control fibroblasts. We cocultured these recipient cells with exosomes purified from the media of control fibroblasts, *Neu1*$^{-/-}$ myofibroblasts, and sialidosis fibroblasts. Notably, we obtained a significant up-regulation of the genes encoding members of the TGF-β and WNT signaling pathways when normal murine or human recipient fibroblasts were cocultured with *Neu1*$^{-/-}$ exosomes or sialidosis-derived exosomes (Fig. 5, D to L, and fig. S7, C and D). This effect was not seen when WT cells were cocultured with exosomes isolated from *Neu1*$^{-/-}$ fibroblast transduced with a lentiviral vector expressing human NEU1 (Fig. 5, D to L), suggesting that reconstituted NEU1 activity in the affected tissue corrected the release of profibrotic exosomes responsible for myofibroblast transdifferentiation. Given the established role of lysosomal-associated membrane protein 1 (LAMP1) in the docking of lysosomes to the PM before engaging in lysosomal exocytosis, we chose to isolate exosomes from *Neu1*/*Lamp1* double-knockout cells. The latter cells showed reduced release of exosomes compared to the *Neu1*$^{-/-}$ myofibroblasts (Fig. 5, D to L), confirming that Lamp1 ablation inhibited lysosomal exocytosis (*14*, *16*). These exosomal preparations fed to WT fibroblasts did not elicit their activation into myofibroblasts to the extent of the *Neu1*$^{-/-}$ exosomes (Fig. 5, D to L). These results prove that NEU1-regulated lysosomal exocytosis is pivotal for the extent of exosomal release and possibly for modulating their cargo. This set of observations, never described in a noncancer setting, identifies exosomes exocytosed in excess by NEU1-deficient cells as strong inducers of a myofibroblast program characteristic of tumor-derived exosomes.

NEU1 is down-regulated in idiopathic pulmonary fibrosis

We next wondered whether *Neu1*$^{-/-}$ mice might represent a naturally occurring model of generalized fibrosis. We therefore performed Masson's trichrome staining in other tissues/organs of the mutant mice, particularly those that are common targets of human fibrosis, such as the lung, liver, and kidney (*29*). The widespread nature of the connective tissue abnormalities was evident in other *Neu1*$^{-/-}$ tissues (fig. S8, A and B). Focusing on the lung fibrosis, frequently occurring in the human population and often of unknown etiology, we compared the levels of *NEU1* mRNA expression in fibroblasts isolated from idiopathic pulmonary fibrosis (IPF) explants (n = 14)

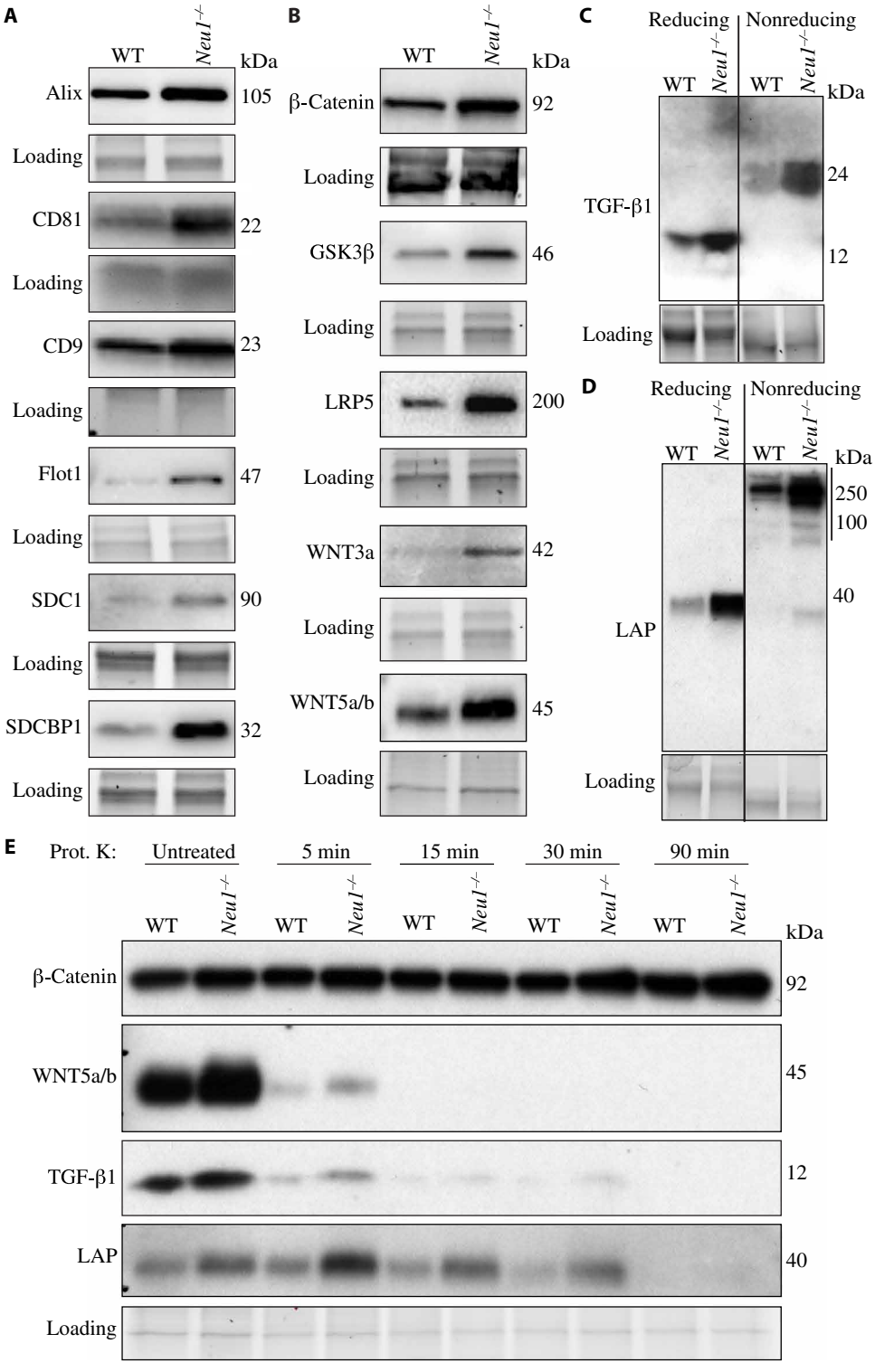

Fig. 4. *Neu1*$^{-/-}$ exosomes contain increased levels of components of the TGF-β and WNT signaling pathways. (**A**) Exosomes exocytosed by *Neu1*$^{-/-}$ myofibroblasts were verified on immunoblots probed with antibodies against established exosomal markers [Alix, CD81, CD9, flottilin-1 (Flot1), Syndecan-1 (SDC1), and syntenin 1 (SDCBP1)]. (**B**) Immunoblot analyses of WT and *Neu1*$^{-/-}$ exosomes performed with antibodies against canonical (β-catenin, GSK3β, LRP5, and WNT3a) and noncanonical (WNT5a/b) WNT signaling. (**C** and **D**) Immunoblots of WT and *Neu1*$^{-/-}$ exosomes probed with anti–TGF-β1 (C) and LAP (D) antibodies. (**E**) Exosomes treated with proteinase K were analyzed on immunoblots probed with anti–TGF-β1, anti-LAP, anti-WNT5a/b, and anti–β-catenin antibodies.

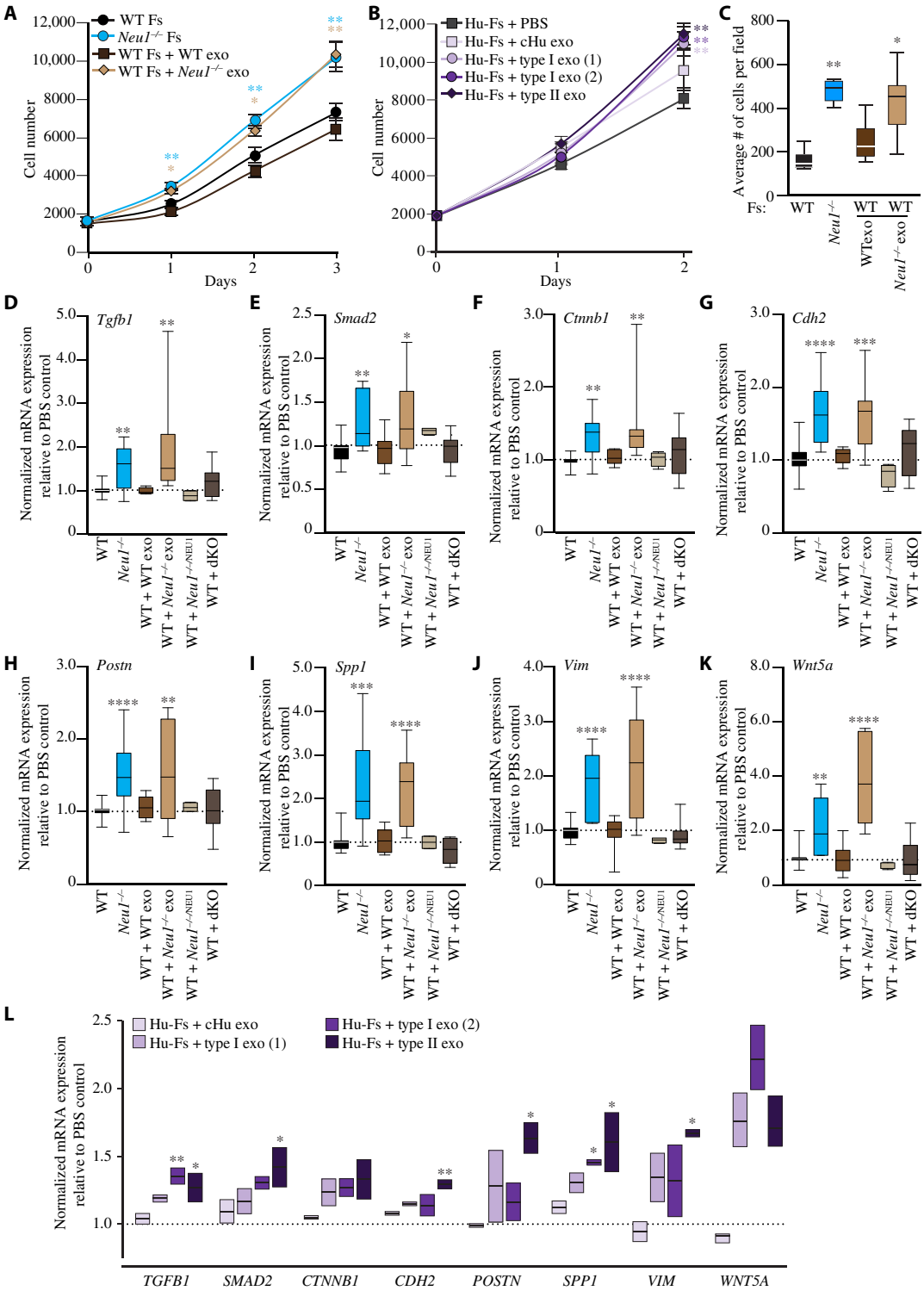

Fig. 5. NEU1-deficient exosomes convert fibroblasts into myofibroblast. (**A** and **B**) Cell proliferation was measured in murine (A) WT fibroblasts (WT Fs) cocultured with murine WT or *Neu1*$^{-/-}$-derived exosomes (exo) ($n = 3$) and in human (B) skin fibroblasts (Hu-Fs) cocultured with exosomes isolated from cultured medium of patients with type I or II sialidosis ($n = 3$). (**C**) Invasive/migratory capacity of murine WT fibroblasts after coculturing them with WT or *Neu1*$^{-/-}$ exosomes ($n = 8$). (**D** to **K**) Increased mRNA expression of markers of the TGF-β and WNT signaling pathways was detected in WT murine fibroblasts (WT) cocultured with *Neu1*$^{-/-}$ exosomes but not with exosomes isolated from pCL20c-*NEU1*–transduced cells (*Neu1*$^{-/-/NEU1}$) or from *Neu1*$^{-/-}$/*Lamp1*$^{-/-}$ cells (dKO) ($n \geq 5$). (**L**) Increased mRNA expression of markers of the TGF-β and WNT signaling pathways in human skin fibroblasts cocultured with human control (cHu), sialidosis type I, or sialidosis type II exosomes ($n = 3$). Normalized (by 18*S* rRNA or *HPRT1*) mRNA expression relative to phosphate-buffered saline (PBS) control. Values are expressed as average ± SD. Statistical analysis was performed using the Student *t* test; *$P < 0.05$, **$P < 0.01$, ***$P < 0.001$, ****$P < 0.0001$.

and WT controls (n = 13). Patients' fibroblasts showed a significantly lower *NEU1* expression (Fig. 6A). This was confirmed by immunofluorescence (IF) staining of NEU1 in a representative cohort (n = 4) of fibroblasts of patients with IPF (Fig. 6B and fig. S8, C and D). To draw a parallel with the muscle-derived *Neu1*$^{-/-}$ myofibroblasts, we also demonstrated enhanced expression of a set of EMT inducers

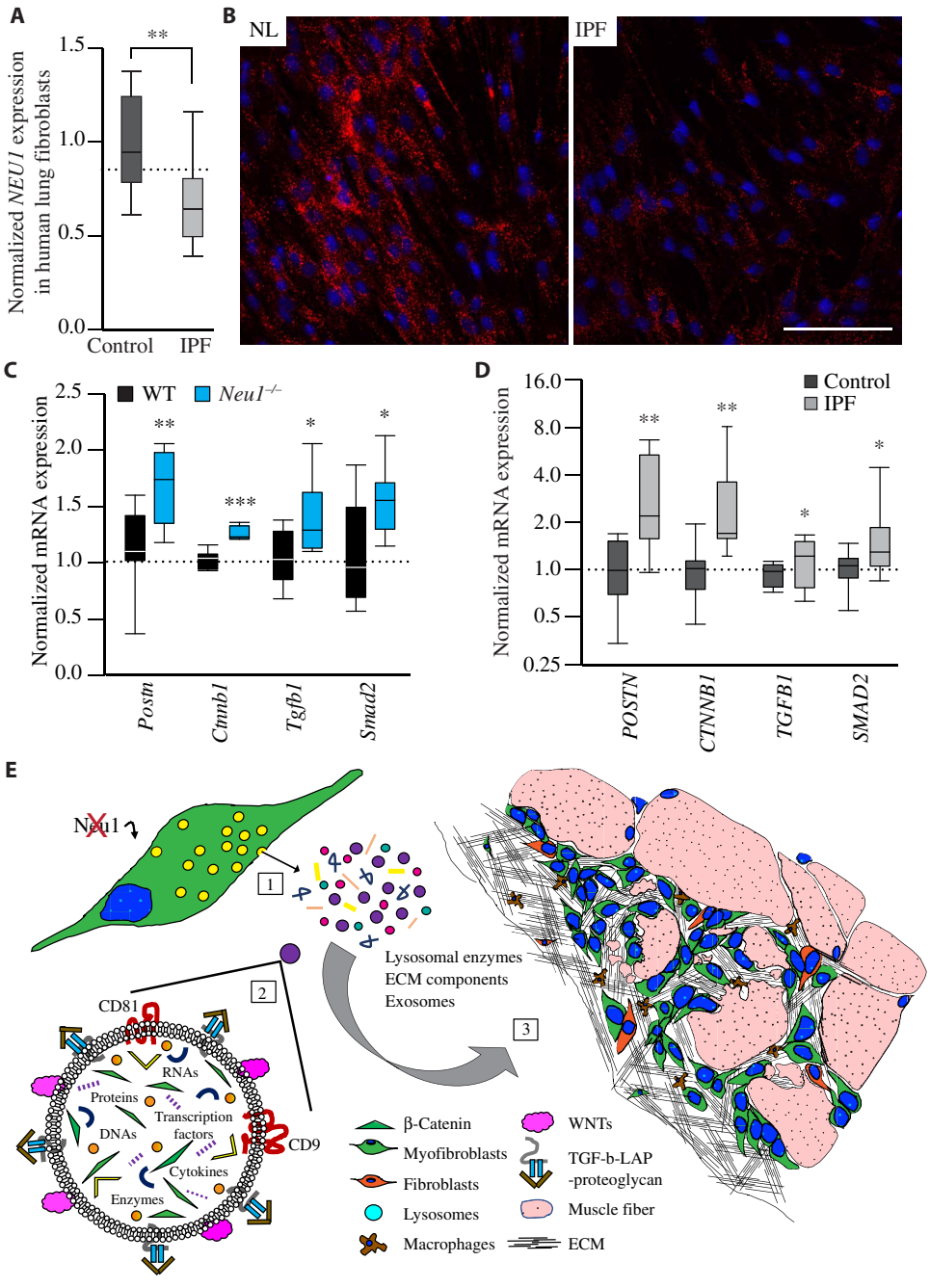

Fig. 6. Down-regulation of *NEU1* correlates with activation of profibrotic signals in IPF fibroblasts. (**A**) RT-qPCR of *NEU1* mRNA in control (n = 13) and IPF (n = 14) patients' fibroblasts. (**B**) Representative IF images of control (NL) and IPF fibroblasts labeled with anti-NEU1 antibody. Scale bar, 100 μm. (**C**) RT-qPCR of *Postn*, *Ctnnb1*, *Tgfb1*, and *Smad2* mRNAs in mouse WT and *Neu1*$^{-/-}$ lung (myo)fibroblasts (n = 5). (**D**) RT-qPCR of *POSTN*, *CTNNB1*, *TGFB1*, and *SMAD2* mRNAs in human control and IPF lung fibroblasts (n = 12). Levels of mRNA expression were normalized by 18*S* rRNA or *GAPDH*. Values are expressed as means ± SD. Statistical analysis was performed using the Student t test; *P < 0.05, **P < 0.01, ***P < 0.001. (**E**) Proposed model of fibrosis induced by NEU1 deficiency. (1) Schematic representation of *Neu1*$^{-/-}$ myofibroblasts that have exacerbated lysosomal exocytosis of soluble lysosomal enzymes and exosomes. (2) Magnification of a *Neu1*$^{-/-}$ exosome containing, among others, increased amounts of activated components of the TGF-β and WNT signaling pathways, responsible for propagating fibrotic signals to neighboring or distant cells. (3) Consequences of excessive lysosomal exocytosis of lysosomal hydrolases and exosomes by *Neu1*$^{-/-}$ myofibroblasts that result in massive ECM degradation/remodeling and full-blown fibrosis leading to myofiber degeneration.

(table S1) in *Neu1*$^{-/-}$ lung fibroblasts compared to WT controls, suggesting that they maintain a myofibroblast phenotype (Fig. 6C). As observed for *Neu1*$^{-/-}$ lung fibroblasts, the mRNA expression of the same EMT effectors (table S1) was enhanced also in IPF lung fibroblasts compared to controls (Fig. 6D), implying a causative effect of NEU1 down-regulation in driving an EMT-like process in this tissue. Collectively, these observations point to NEU1 deficiency/down-regulation as potential risk factor for the development of a fibrotic disease.

DISCUSSION

Fibrosis is defined as the formation of fibrous connective tissue in damaged or injured organs that occurs during normal wound healing or in response to a wide range of pathological insults, including inflammation, infections, or cancer (*30*). However, many fibrotic conditions in humans are still of unknown etiology (*30*). A general feature of fibrosis is the activation of fibroblasts into myofibroblasts, cells with mesenchymal characteristics that play a central role in the secretion/remodeling of the ECM, altering the stiffness and composition of the tissue in an autocrine and/or paracrine way (*3*, *31*). Dissecting the molecular mechanisms that initiate and sustain the differentiation and transformation of resident cells into proliferating and ECM-producing myofibroblasts is vital for tackling idiopathic forms of fibrosis mechanistically and therapeutically.

Here, we have made the notable and unexpected discovery that deficiency of the sialic acid processing enzyme NEU1, linked to the rare pediatric lysosomal disease sialidosis, triggers the relentless expansion of the connective tissue, leading to a full-blown fibrosis (Fig. 6E). We also demonstrate down-regulation of NEU1 in a cohort of human IPF fibroblasts, suggesting a role for NEU1 deficiency/down-regulation in causing or hastening the course of a fibrotic disease in the adult human population. Although seemingly in contrast with previously published literature (*32*, *33*), our findings are in full agreement with the results of RNA sequencing, covering 66 genes encompassing the human leukocyte antigen chromosomal region, performed in lung tissue of 87 patients with IPF (*34*). In this dataset, *NEU1* ranked as one of the top down-regulated genes.

Mechanistically, we show that the pathogenic process leading to the fibrotic disease in the sialidosis mice and likely in the corresponding human disease is initiated and perpetuated by the relentless, excessive lysosomal exocytosis of NEU1-deficient myofibroblasts. These cells release a high load of harmful lysosomal hydrolases (i.e., cathepsins) that degrade the ECM (*35*) and a high yield of exosomes, laden with TGF-β and WNT signaling molecules that fuel the fibrotic process. We demonstrate that in the absence of NEU1, cells of the skeletal muscle connective tissue have all features of myofibroblasts and maintain a status of transdifferentiation resembling an EMT/MET process, also known as "metastable" phenotype, which was shown to occur in the aggressive forms of sarcoma (*36*). Thus, NEU1 deficiency/down-regulation may create the appropriate setting to study cells trapped in this intermediate state, which have been notoriously difficult to characterize.

The mechanisms that generate myofibroblasts are not fully understood. Multiple lineage tracing and genetic studies have identified several precursor cells of myofibroblasts, including MPs and FAPs (*4*). The latter were shown to differentiate into ectopic adipocytes and/or fibroblasts and, in turn, become myofibroblasts in the skeletal muscle (*37*). However, both MPs and FAPs are not the source of myofibroblasts in our model, but rather, they originate from self-activating resident fibroblasts, which acquire the capacity to propagate fibrotic signals to neighboring cells via excessive exocytosis of exosomes. This increased number of released exosomes downstream of NEU1 deficiency could be explained by either preferential docking of multivesicular bodies (MVBs) at the PM poised to exocytose their contents or by constant fusion of already PM-docked lysosomes with MVBs, immediately preceding lysosomal exocytosis. In addition, it is conceivable that exacerbation of lysosomal exocytosis and consequent redistribution of lysosomal membrane components at the PM create "exocytic" membrane microdomains that may further favor the docking and fusion of endolysosomes at the PM. These pathogenic sequelae have never been observed in a noncancer setting and are the consequence of NEU1's control over the pool of endolysosomes that relocate to the PM.

Although exosomes have been implicated in cancer progression (*38*), their involvement in eliciting a fibrotic condition in a pediatric lysosomal disease was unknown until now. We present evidence for the first time that exosomes from NEU1-deficient myofibroblasts can change the phenotype of normal cells, educating them to acquire myofibroblast characteristics. This pernicious circle is initiated and maintained by the concomitant induction of TGF-β and both canonical and noncanonical WNT signaling pathways (*10*, *36*). Cross-talk between these two pathways has been confirmed in animal models of fibrosis (*39*). These authors showed that canonical WNT signaling is required for TGF-β–mediated fibrosis because transgenic overexpression of a WNT inhibitor dampens the activity of TGF-β (*39*). On the other hand, the induction of TGF-β results in the stabilization of the cytosolic β-catenin and the activation of its downstream target genes (*40*). We hypothesize that coactivation of these pathways in Neu1-deficient myofibroblasts favors the establishment and maintenance of an intermediate/metastable EMT-like program and the development of the fibrotic process.

As previously described in exosomes isolated from cancer cells (*28*), we found that both TGF-β in its latent form and noncanonical WNT5a/b ligands are associated with the outer membrane site of *Neu1*$^{-/-}$ exosomes, probably bound to heparan sulfate proteoglycans, such as glypicans. The latter, known to be required for efficient TGF-β and WNT signaling (*41*, *42*), are also strongly up-regulated in *Neu1*$^{-/-}$ exosomal preparations (table S2). The topological configuration of these TGF-β and WNT ligands may support maximal activation of their respective signaling cascades. On the basis of these results, we can infer that exosomes from NEU1-deficient myofibroblasts direct cells to obtain characteristics of a precancerous state. Consistent with this hypothesis is the finding that *Neu1* haploinsufficiency in a tumor-prone mouse model is sufficient to foster the development of invasive/metastatic, pleomorphic sarcomas, baring both epithelial and mesenchymal features (*16*).

The simultaneous up-regulation of WNT3a and WNT5a/b in exosomes reconciles the proliferative and migratory characteristics of *Neu1*$^{-/-}$ myofibroblasts and explains the acquisition of these same features by control fibroblasts cocultured with *Neu1*$^{-/-}$ exosomes. It has been demonstrated that up-regulation of noncanonical WNT5a synergizes with the canonical pathway during the EMT process (*43*). However, up-regulation of WNT5a has also been linked to the occurrence of human IPF by inducing proliferation independently of the canonical WNT/β-catenin pathway (*44*).

In conclusion, we provide evidence that NEU1 functions as a modulator of fibrosis in the skeletal muscle and other tissues of the

Neu1$^{-/-}$ mice, a feature that not only justifies characteristic symptoms of sialidosis in patients but also is applicable to other common conditions, such as idiopathic fibrosis and cancer. Last, because NEU1 levels are decreased in some forms of IPF, *NEU1* down-regulation may represent a risk factor for the initiation and/or progression of the fibrotic disease. It is tantalizing to hypothesize that NEU1 expression levels may be of prognostic value for human forms of fibrosis for which there is currently no treatment.

MATERIALS AND METHODS

Experimental design

The main goal of this study was to dissect the molecular mechanism(s) downstream of NEU1 deficiency responsible for the generalized fibrosis characteristic of *Neu1*$^{-/-}$ mice, focusing on the muscle connective tissue. All biochemical experiments described in this manuscript were repeated at least three times, including immunohistochemical (IHC) analyses, FACS, proliferation assays, invasion/migration assays, IF analyses, immunoblots, and RT-qPCR.

In a previous study, we reported the observation that *Neu1*$^{-/-}$ mice develop a progressive expansion of the muscle connective tissue with massive deposition of ECM. Therefore, we first analyzed the cell population(s) responsible for this connective tissue expansion and determined by FACS analysis that 95% of the cells were myofibroblasts. We further demonstrated that *Neu1*$^{-/-}$ myofibroblasts maintained a semidifferentiated status, namely, they were not only highly proliferative but also invasive and migratory, and produced and secreted profibrotic signals, such as TGF-β, as determined by IHC, IF, and Western blot (WB) analyses. These features of the *Neu1*$^{-/-}$ muscle connective tissue could be reverted completely by intravenous injection of recombinant AAV vectors expressing NEU1 and its auxiliary protein PPCA.

The aforementioned characteristics of the *Neu1*$^{-/-}$ myofibroblasts resembled those observed in aggressive sarcoma and known as metastable/intermediate EMT/MET (*25*, *36*). We tested this hypothesis by probing an EMT-PCR array containing ECM and profibrotic molecules, followed by validation of the data with RT-qPCRs. The results of these experiments confirmed up-regulation of the TGF-β signaling pathway and revealed the concomitant activation of several components of canonical and noncanonical WNT signaling pathways. To further define the mode of propagation and amplification of these profibrotic signals, we tested the components expelled extracellularly by *Neu1*$^{-/-}$ myofibroblasts, known to have exacerbated lysosomal exocytosis of active hydrolytic enzymes as consequence of Neu1 deficiency. We found that besides increased exocytosis of lysosomal cathepsins responsible for degrading the ECM, *Neu1*$^{-/-}$ myofibroblasts also exocytosed increased number of exosomes. Purified nanovesicles from the medium of *Neu1*$^{-/-}$ myofibroblasts were extensively characterized using electron microscopy (EM), comparative high-throughput proteomics, and immunoblot techniques. These analyses revealed that *Neu1*$^{-/-}$-purified exosomes were loaded with molecules of the TGF-β and WNT signaling pathways. The increased levels of these molecules in *Neu1*$^{-/-}$ exosomes led us to investigate whether these nanovesicles were directly involved in the rapid propagation of fibrotic signals from cell to cell. We tested this hypothesis by coculturing murine and human WT fibroblasts with purified exosomes from murine WT fibroblasts and *Neu1*$^{-/-}$ myofibroblasts or from fibroblasts of patients with sialidosis. By performing proliferation, migration/invasion assays, and gene expression profiling on the recipient fibroblasts, we demonstrated that mouse- or patient-derived Neu1-deficient exosomes had the capacity to transform WT fibroblasts into myofibroblasts and thereby to propagate and expand the fibrotic signals from cell to cell. These findings establish a role for NEU1 in the regulation of exosome release and define the molecular network responsible for the initiation and maintenance of a fibrotic process.

Last, to directly address the potential involvement of NEU1 in human fibrosis, we first determined by Masson's trichrome staining that the fibrotic disease seen in the muscle was a general phenotype of the *Neu1*$^{-/-}$ connective tissue in different organs. We then analyzed fibroblasts isolated from lungs of patients with IPF and compared their gene expression profiles with those of *Neu1*$^{-/-}$ lung fibroblasts using RT-qPCR and IF staining. Combined, our results point to *Neu1*$^{-/-}$ mice as a potentially suitable model of generalized fibrosis and suggest that NEU1 levels may hold prognostic value for human fibrosis.

Animals

WT and *Neu1*$^{-/-}$ mice age 1 to 5 months (FVB/NJ background) (*20*), and the *Lamp1*$^{-/-}$ mouse (*45*), a gift from Dr. Paul Saftig and was crossed with the *Neu1*$^{-/-}$ mouse, were included in this study. Animals were housed in a fully AAALAC (Assessment and Accreditation of Laboratory Animal Care)–accredited animal facility with controlled temperature (22°C), humidity, and lighting (alternating 12-hour light/dark cycles). Food and water were provided ad libitum. All procedures in mice were performed according to animal protocols approved by the St. Jude Children's Research Hospital Institutional Animal Care and Use Committee and National Institutes of Health guidelines.

Antibodies

We used the following commercial antibodies for IF, IHC, and WB analyses: anti–TGF-β (3709, Cell Signaling; IHC, 1:100; WB, 1:1000), anti–TGF-β1 (sc-130348, Santa Cruz Biotechnology; IF, 1:25), anti-Smad2 (5339, Cell Signaling; IHC, 1:50; WB, 1:1000), anti-pSmad2 (3108, Cell Signaling; IHC, 1:50; WB, 1:1000), anti-vimentin (20R-VP004, Fritzgerald; IF, 1:250; WB, 1:2000), anti–collagen IV (2150-1470, AbD Serotec; IF, 1:100; WB, 1:1000), anti–β-catenin (610154, BD Biosciences; IF, 1:25), anti–β-catenin (8480, Cell Signaling; WB, 1:1000), anti–collagen Iα1 (NB600-408, Novus Biological; IF, 1:500; WB, 1:5000), E-cadherin (3199, Cell Signaling; IF, 1:100; WB, 1:1000), anti-αSMA [C6198 αSMA-CY3 or F3777 αSMA-FITC (fluorescein isothiocyanate), Sigma-Aldrich; IF, 1:100; WB, 1:1000], anti–TCF4-488 (05-511-AF488, MilliporeSigma; IF, 1:100), anti-TCF4/TCF7L2 (2569, Cell Signaling; WB, 1:1000), anti-periostin (sc-67233, Santa Cruz Biotechnology; IF, 1:50; WB, 1:250), anti-osteopontin (AF808, R&D Systems; IHC, 1:25; WB, 1:250), anti-ALIX (generated in d'Azzo laboratory; WB, 1:300), anti-CD81 (sc-166029, Santa Cruz Biotechnology; WB, 1:250), anti-CD9 (553758, BD Biosciences; WB, 1:500), anti–flotillin-1 (610820, BD Biosciences; WB, 1:500), anti–syndecan-1 (36-2900, Life Technologies; WB, 1:250), anti–syntenin-1 (AB15272, Thermo Fisher Scientific; WB, 1:500), anti-GSK3β (9315, Cell Signaling; WB, 1:1000), anti-LRP5 (5731, Cell Signaling; WB, 1:1000), anti-WNT3a (sc-28472, Abcam; WB, 1:500), anti-WNT5a/b (2530, Cell Signaling; WB, 1:1000), anti-human LAP (AF-246-NA, R&D Systems; WB, 1:500), and anti-human NEU1 (d'Azzo laboratory; IF, 1:50). CY3-, FITC-, 488-, and horseradish peroxidase (HRP)–conjugated secondary antibodies were purchased from Jackson ImmunoResearch Laboratory (West Grove, PA); 488-conjugated secondary antibodies were from Molecular Probes.

Murine and human fibroblasts cultures

Skeletal muscles were collected from WT and *Neu1*$^{-/-}$ mice, digested with a mixture of collagenase P (5 mg/ml; Roche), dispase II (1.2 U/ml; Roche), and $CaCl_2$ (5 mM; Thermo Fisher Scientific) in phosphate-buffered saline (PBS) at 37°C for 45 min, and mixed every 10 min. Dulbecco's modified Eagle's medium (DMEM)–primary calf serum (PCS) complete medium [10% PCS (Fisherbrand), penicillin (100 U/ml), streptomycin (100 μg/ml) (Gibco), and 2 mM GlutaMAX (Gibco)] was added to the digested muscle, the mixture was filtered and spun down, and the cells seeded into 10-cm dishes and incubated at 37°C/5% CO_2/3% O_2. Fibroblasts were cultured to 100% confluency for passage P0 and to 80% for further passages. The skin of *Neu1*$^{-/-}$/*Lamp1*$^{-/-}$ mice was naired and cleaned with ethanol, and a small square piece was collected in cold PBS. The piece was cut into 1-mm fragments and cultured in DMEM-PCS at 37°C/5% CO_2 to outgrow the fibroblasts. The cells were further expanded as described above.

Human skin fibroblasts from control individuals were obtained from Coriell Institutes; skin fibroblasts from patients with type I and type II sialidosis were available in our laboratory. The cells were cultured and maintained in DMEM–fetal bovine serum (FBS)–complete medium [containing 10% FBS (Biowest)] at 37°C/5% CO_2. Cells were grown to 80 to 90% confluency before passaging.

Human lung fibroblasts from control individuals and patients with IPF were obtained as previously described (*46*). The cells were cultured and maintained in DMEM-FBS complete medium containing sodium pyruvate at 37°C/5% CO_2. Cells were grown to 80 to 90% confluency before passaging.

Masson's trichrome staining

Masson's trichrome staining was performed following the manufacturer's protocol (Polysciences Inc.). The muscle tissues were fixed in 10% buffered formalin and embedded in paraffin. Transverse sections of the muscle were cut (6 μm), deparaffinized, and fixed in Mordant in Bouin's solution for 1 hour at 60°C. Sections were stained sequentially at room temperature with Weigert's iron hematoxylin, Biebrich scarlet-acid fuchsin, phosphotungstic/phosphomolybdic acid, and aniline blue. Sections were washed, dehydrated, and mounted with a xylene-based mounting medium.

Fluorescence-activated cell sorting

FACS analyses of skeletal muscle connective tissue cells were performed using markers specific for MPs, FAPs, and myofibroblasts on a flow cytometer instrument (4 BD Biosciences LSR/Fortessa instrument). Whole skeletal muscles were dissected from mice (age 2 to 5 months) and kept on ice. The muscles were then shredded manually and incubated with collagenase II (Sigma-Aldrich) and $CaCl_2$ for 30 min at 37°C. Ice-cold PBS was added, and the mixture was centrifuged at 1600 rpm for 5 min. Cell pellets were resuspended in a mixture of collagenase D (Roche), dispase II (Roche), and $CaCl_2$ and incubated at 37°C, rotating for 1 hour. After addition of ice-cold PBS, the mixture was filtered using a 40-μm cell strainer and centrifuged at 1600 rpm for 5 min at 8°C, and the pellet was resuspended in 1-ml ice-cold PBS and 2% FBS. FACS analyses of MPs and FAPs were performed using anti-CD31–FITC (553372, BD Biosciences), anti-CD45–FITC (553080, BD Biosciences), anti-Sca–PECY7 (25-5981-82, eBioscience), and anti–integrin-α7–APC (FAB3518A, R&D Systems) antibodies. The MP cell population was selected for CD45$^-$, CD31$^-$, (all leucocytes, endothelial cells, and platelets), Sca1$^-$, and integrin-α7$^+$. The FAP cell population was selected for CD45$^-$, CD31$^-$, Sca1$^+$, and integrin-α7$^-$. For fibroblasts and myofibroblasts, cells were stained with anti-CD31–BV421 (562939, BD Biosciences) or anti-CD31–APC (11-0311-82, eBioscience), anti-CD45–eVolve-605 (83-0451-42, eBioscience) or anti-CD45–APC (17-0451-82, eBioscience), anti-TCF4–Alexa Fluor 488 (05-511-AF488, Sigma-Aldrich), and anti-αSMA–CY3 (C6198, Sigma-Aldrich) antibodies and selected for CD45$^-$, CD31$^-$, TCF4$^+$, and αSMA$^-$ or CD45$^-$, CD31$^-$, TCF4$^+$, and αSMA$^+$, respectively.

Proliferation assay

Cells' growth rate was measured by 3-(4,5-dimethylthiazol-2-yl)-5-(3-carboxymethoxyphenyl)-2-(4-sulfophenyl)-2*H*-tetrazolium, inner salt staining (MTS; Promega). Murine WT, *Neu1*$^{-/-}$ cells, and human skin fibroblasts were synchronized by treatment with nocodazole (100 ng/ml; Sigma-Aldrich) for 16 hours at 37°C/5% CO_2 or 37°C/5% CO_2/3% O_2. Cells were collected, counted, and seeded at 1500 to 2000 cells per well in a 96-well plate. Proliferation assay was performed every 24 hours for 1 to 4 days by adding 20 μl of MTS solution to each well and incubating the cells for 2 hours. The optical density was read at 490 nm (OD_{490}) with a plate reader (FLUOstar Omega, BMG LABTECH). In addition, cells were co-cultured with murine or human exosomes (25 to 50 μg/ml) or equal volume of PBS, and cell growth was measured at days 1 to 3 of culture.

Invasion/migration assays

Fibroblasts' invasion/migration assays were carried out in BD BioCoat Matrigel Invasion Chambers (Corning) containing an 8-μm-pore–size PET (polyethylene terephthalate) membrane with a thin layer of Matrigel basement membrane matrix according to the manufacturer's protocol. WT and *Neu1*$^{-/-}$ (myo)fibroblasts (62.5×10^3) were seeded in the upper well without attractant and cultured for 22 hours at 37°C/5% CO_2. The noninvading cells were removed from the upper surface of the membrane that was then fixed in methanol, stained with toluidine blue, washed, and air-dried. Migrated cells were counted from three separate experiments (four fields per membrane). WT murine fibroblasts were cocultured with WT or *Neu1*$^{-/-}$ exosomes (20 μg/ml), and their migratory capacity was assayed as described above.

The ex vivo basement membrane invasion assay was conducted as follows: The peritonea from 8- to 12-week-old FVB mice were mounted over 6.5-mm Transwell inserts (Thermo Fisher Scientific). Peritoneum constructs were then treated with 1 M ammonium hydroxide for 1 hour and washed extensively. A total of 5×10^5 WT or *Neu1*$^{-/-}$ (myo)fibroblasts were cultured on top of WT or *Neu1*$^{-/-}$ peritonea cultured ex vivo in DMEM-PCS complete medium for 12 days. Fresh medium (200 μl) was applied every day to each insert. Peritonea were fixed in buffered formalin, cross-sectioned, and hematoxylin and eosin–stained. The average number of invading cells per peritonea was counted in 12 adjacent sections encompassing the entire length of the peritonea from four separate experiments.

Cell transduction

Neu1$^{-/-}$ myofibroblasts were transduced with a lentiviral vector expressing the human NEU1 gene (pCL20c-*NEU1*-puro); stable cell clones were selected with puromycin (1 μg/ml). As control, *Neu1*$^{-/-}$ myofibroblasts were transduced with a pCL20c–YFP (yellow fluorescent protein) vector and selected for YFP expression. The latter cells maintained the characteristics of not transduced knockout cells with regard to the extent of exosome release.

Real-time quantitative polymerase chain reaction

Total RNA was isolated from WT and *Neu1*$^{-/-}$ GA skeletal muscles (1, 3.5, and 5 months) and human and murine (myo)fibroblasts using the PureLink RNA Kit (Life Technologies) according to the manufacturer's protocol. DNA contaminants were removed on a deoxyribonuclease I column (Life Technologies), according to the manufacturer's protocol. RNA quantity and purity were measured using NanoDrop Lite spectrophotometer (Thermo Fisher Scientific). Complementary DNA was produced using 0.5 to 5 μg of total RNA with RT^2 First Strand Kit (QIAGEN). RT-qPCR was performed using RT^2 SYBR Green qPCR Mastermix, 1 μl (8, 16, or 50 ng) of complementary DNA, 10 μM primer, and ribonuclease-free water in a 25-μl reaction volume on an iQ5 or CFX96 real-time PCR machine (Bio-Rad). Samples were normalized to 18*S* ribosomal RNA (murine), *GAPDH*, or *HRTP1* (human). The specific mouse and human primers used are summarized in table S1.

For RNA isolation of murine WT fibroblasts or human control skin fibroblasts cocultured with exosomes, 2.5×10^5 cells were seeded in 10-cm dishes. Murine WT, *Neu1*$^{-/-}$, *Neu1*$^{-/-}$/*Lamp1*$^{-/-}$ and *Neu1*$^{-/-/NEU1}$ (pCL20c-*NEU1*-puro) exosomes, human control, or sialidosis type I or type II exosomes (50 to 70 μg) were added to the dish at days 0 and 1, and cell pellets were collected on day 3 and stored at −80°C until use.

Immunohistochemistry and IF

For IHC analysis, muscle tissues were fixed in 10% buffered formalin and embedded in paraffin. Transverse sections of the muscle were cut (6 μM) and deparaffinized, and antigen retrieval was performed using citrate buffer [0.1 M citric acid and 0.1 M sodium citrated (pH 6.0) containing 0.05% Tween 20]. The sections were blocked in PBS, 10% normal donkey serum, 0.1% bovine serum albumin (BSA) and 0.5% Tween 20 or with malate buffer, 20% CCS (cosmic calf serum), and 2% blocking solution (Roche) and incubated overnight with primary antibodies. Sections were incubated with biotinylated secondary antibodies for 1 hour, and endogenous peroxidase was removed using 0.1% H_2O_2 for 30 min. Antibody signal was detected using the ABC (Avidin-Biotin Complex) Kit and diaminobenzidine substrate (Vector Labs), and the sections were counterstained with hematoxylin or methyl green according to the standard protocols.

For IF staining, the skeletal muscles from WT and *Neu1*$^{-/-}$ mice were dissected, mounted in tissue-freezing medium (Triangle Biomedical Sciences Inc.) or placed on cork containing tragacanth (Sigma-Aldrich), frozen immediately in isopentane cooled in liquid nitrogen, and stored at −80°C. Transverse sections (8 μM) were cut on a cryostat (Leica CM3050) and fixed/permeabilized with 1% paraformaldehyde (PFA), 0.2% saponin, or 0.1% Triton X-100 in PBS for 20 min. Preincubation of sections with AffiniPure Fab Fragment Goat Anti-Mouse Immunoglobulin G (H + L) was performed to reduce cross-reactivity when monoclonal antibodies were used. Sections were incubated with Image-iT FX Signal Enhancer (Life Technologies), blocked with 10% normal donkey serum, 0.1% BSA, and 0.5% Tween 20 in PBS, and incubated overnight with primary antibodies. Sections were incubated with fluorophore-conjugated secondary antibodies, washed, dried, and mounted with ProLong Gold antifade reagent with 4′,6-diamidino-2-phenylindole (DAPI; Life Technologies).

For IF stainings, human control and IPF lung fibroblasts were seeded at a confluency of 5×10^4 per well (Nunc Lab-Tek II Chamber Slide, four-well slide; Thermo Scientific Nunc). Fibroblasts were washed 3× with ice-cold PBS, fixed in precooled (−20°C) 95% ethanol/5% acetic acid for 10 min, and washed 2× in ice-cold PBS. ImageIT was used to intensify the staining. The cells were incubated overnight with primary antibody diluted in blocking buffer [25 mM Na-Phosphate (pH 7.5), 150 mM NaCl, 1% BSA, and 0.3% gelatin]. The slides where washed three times in blocking buffer, incubated with a fluorophore-conjugated secondary antibody, washed, dried, and mounted with ProLong Gold antifade reagent with DAPI (Life Technologies). The cells were imaged on a confocal microscope (Nikon C1si or C2; Zeiss LSM 780).

WB analysis

Skeletal muscles from WT, *Neu1*$^{-/-}$, and *Neu1*$^{-/-}$ mice injected with scAAV2/8-NEU1 (2×10^{11} vector genomes) and scAAV2/8-PPCA (1×10^{11} vector genomes) were grinded till powder in liquid nitrogen and homogenized in 10 (w/v) radioimmunoprecipitation assay (RIPA) buffer (0.1% SDS, 1% sodium deoxycholate, 1% Triton X-100, 140 mM NaCl, 10 mM tris, protease inhibitors cocktail, and phosphatase inhibitors) or in PBS or in double-distilled H_2O using an Omni Prep Multi-Sample homogenizer 2 × 2 min at 30 Hz. WT and *Neu1*$^{-/-}$ (myo)fibroblasts pellets were lysed in RIPA or PBS. The protein concentration was determined by OD_{595} using BSA solution (Pierce). Each protein sample (5 to 50 μg) underwent electrophoresis on NuPAGE Novex (4 to 12, 10, or 12%) bis-tris mini protein gels (Life Technologies) or Criterion TGX Stain-Free precast gels (10 or 12%; Bio-Rad). Gels were wet-blotted against polyvinylidene difluoride membranes and blocked in tris-buffered saline containing 0.1% Tween 20 (TBS-T) and 5% nonfat dry milk. The membranes were incubated overnight at 4°C with primary antibodies in either 3% BSA–TBS-T solution or 5% milk in TBS-T. The next day, membranes were incubated with HRP-conjugated secondary antibodies and developed using SuperSignal West Femto Maximum Sensitivity Substrate (Thermo Fisher Scientific). Quantitative analyses of the WBs were performed with Image Lab software.

Exosome isolation, sucrose gradient, proteomics, and size distribution

Exosomes were purified from the conditioned media of murine fibroblasts isolated from the skeletal muscle or the skin of WT, *Neu1*$^{-/-}$, and *Neu1*$^{-/-}$/*Lamp1*$^{-/-}$ mice. In addition, exosomes were purified from the conditioned media of *Neu1*$^{-/-}$ myofibroblasts transduced with lentiviral vectors expressing either the human *NEU1* gene or YFP. Last, exosomes were purified from the media of human skin control fibroblasts and sialidosis type I and type II skin fibroblasts. Fibroblasts were cultured in DMEM-PCS-complete or DMEM-FBS complete medium depleted from contaminating vesicles by ultracentrifugation for 16 hours at 100,000*g* (SW32 Ti rotor, Optima XPN-90, Beckman Coulter). Cultured medium was collected between 18 and 24 hours, and exosomes were purified by sequential centrifugation steps at 300*g* for 10 min, 2000*g* for 10 min, and 10,000*g* for 30 min to remove cells and cell debris. The medium was then ultracentrifuged at 100,000*g* for 2 hours (SW32Ti rotor), and exosomes were washed once with cold PBS and ultracentrifuged at 100,000*g* (SW32Ti rotor) for 2 hours. All steps were performed at 4°C. Exosome pellets were resuspended in ice-cold PBS and used immediately or stored at −80°C.

WT and *Neu1*$^{-/-}$ exosomes were subjected to further purification on a sucrose density gradient. Exosomal pellets were resuspended in 0.25 M sucrose and loaded onto a step gradient of 2 to 0.25 M sucrose in 10 mM tris-HCl buffer (pH 7.4) and 1 mM $Mg(Ac)_2$.

The gradients were ultracentrifuged at 100,000*g* for 2.5 hours in a Beckman Coulter SW41Ti rotor. Twelve 1-ml fractions were collected, and the density was measured using a refractometer (Thermo Fisher Scientific). The Brix° was converted to density in grams per milliliter. The proteins were precipitated with trichloroacetic acid buffer (110 μl of 100%). Pellets were resuspended in NuPAGE lithium dodecyl sulfate sample buffer (Life Technologies or Bio-Rad) with or without 1,4-dithiothreitol and used for WB analyses.

Purified exosomes were subjected to mass spectrometry and analyzed with MaxQuant. Exosome size distribution was determined by measuring the width of exosomes per EM pictures.

Proteinase K treatment of exosomes

Exosomes were subjected to proteinase K treatment to gently remove surface proteins maintaining the vesicles intact. Briefly, 20 μg of isolated WT and *Neu1*$^{-/-}$ exosomes were incubated with proteinase K (50 μg/ml) for 0, 5, 15, 30, and 90 min at 37°C. The reactions were stopped by adding 5 mM phenylmethylsulfonyl fluoride for 10 min at room temperature. Samples were then ultracentrifuged for 2 hours at 100,000*g* at 4°C, and the pellets were subjected to immunoblots probed with anti-WNT5a/b, anti–TGF-β, anti-LAP, and anti–β-catenin antibodies.

EM of exosomes

For the ultrastructural studies, exosome pellets were fixed and embedded using standard protocols (*15*). Briefly, exosome pellets (5 μg) were fixed with 2% PFA and deposited on to Formvar/carbon–coated EM grids (EMS; FCF200-Cu). The grids were washed in PBS, fixed with 1% glutaraldehyde, and washed with distilled water. The samples were contrasted with methyl cellulose:uranyl oxalate solution (0.9:0.5%) and visualized using a JEOL-JEM 1200EX II electron microscope and a Gatan 782 digital camera.

Statistical analyses

Statistical analyses were performed with a two-tailed unpaired Student *t* test using GraphPad Prism. The data are presented as means or averages ± SD. The values of $P < 0.05$ were considered statistically significant.

SUPPLEMENTARY MATERIALS

Supplementary material for this article is available at http://advances.sciencemag.org/cgi/content/full/5/7/eaav3270/DC1

Fig. S1. *Neu1*$^{-/-}$ muscles have increased levels of TGF-β and WNT signaling components.
Fig. S2. *Neu1*$^{-/-}$ muscles show increased levels of periostin and osteopontin.
Fig. S3. WB analyses of WT and *Neu1*$^{-/-}$ (myo)fibroblast lysates.
Fig. S4. *Neu1*$^{-/-}$ muscle and myofibroblasts up-regulate canonical markers that drive an EMT process.
Fig. S5. Characterization of WT and *Neu1*$^{-/-}$ exosomes.
Fig. S6. *Neu1*$^{-/-}$ exosomes contain increased levels of components of the TGF-β and WNT signaling pathways.
Fig. S7. NEU1-deficient exosomes induce a fibroblast to myofibroblast program in recipient normal fibroblasts.
Fig. S8. General fibrosis in the *Neu1*$^{-/-}$ mouse model and decreased NEU1 protein levels in IPF fibroblasts.
Table S1. Murine and human RT-qPCR primers.
Table S2. Comparative high-throughput proteomic analyses of *Neu1*$^{-/-}$ and WT exosomes.

REFERENCES AND NOTES

1. C. Bonnans, J. Chou, Z. Werb, Remodelling the extracellular matrix in development and disease. *Nat. Rev. Mol. Cell Biol.* **15**, 786–801 (2014).
2. P. M. Gilbert, V. M. Weaver, Cellular adaptation to biomechanical stress across length scales in tissue homeostasis and disease. *Semin. Cell Dev. Biol.* **67**, 141–152 (2017).
3. R. T. Kendall, C. A. Feghali-Bostwick, Fibroblasts in fibrosis: Novel roles and mediators. *Front. Pharmacol.* **5**, 123 (2014).
4. B. Hinz, Myofibroblasts. *Exp. Eye Res.* **142**, 56–70 (2016).
5. A. Uezumi, T. Ito, D. Morikawa, N. Shimizu, T. Yoneda, M. Segawa, M. Yamaguchi, R. Ogawa, M. M. Matev, Y. Miyagoe-Suzuki, S. Takeda, K. Tsujikawa, K. Tsuchida, H. Yamamoto, S. I. Fukada, Fibrosis and adipogenesis originate from a common mesenchymal progenitor in skeletal muscle. *J. Cell Sci.* **124**, 3654–3664 (2011).
6. X. M. Meng, D. J. Nikolic-Paterson, H. Y. Lan, TGF-β: The master regulator of fibrosis. *Nat. Rev. Nephrol.* **12**, 325–338 (2016).
7. J. C. Gross, M. Boutros, Secretion and extracellular space travel of Wnt proteins. *Curr. Opin. Genet. Dev.* **23**, 385–390 (2013).
8. I. Ackers, R. Malgor, Interrelationship of canonical and non-canonical Wnt signalling pathways in chronic metabolic diseases. *Diab. Vasc. Dis. Res.* **15**, 3–13 (2018).
9. A. Kikuchi, H. Yamamoto, A. Sato, Selective activation mechanisms of Wnt signaling pathways. *Trends Cell Biol.* **19**, 119–129 (2009).
10. S. Lamouille, J. Xu, R. Derynck, Molecular mechanisms of epithelial-mesenchymal transition. *Nat. Rev. Mol. Cell Biol.* **15**, 178–196 (2014).
11. P. Lu, K. Takai, V. M. Weaver, Z. Werb, Extracellular matrix degradation and remodeling in development and disease. *Cold Spring Harb. Perspect. Biol.* **3**, a005058 (2011).
12. G. Rackov, N. Garcia-Romero, S. Esteban-Rubio, J. Carrión-Navarro, C. Belda-Iniesta, A. Ayuso-Sacido, Vesicle-mediated control of cell function: The role of extracellular matrix and microenvironment. *Front. Physiol.* **9**, 651 (2018).
13. A. Rodriguez, P. Webster, J. Ortego, N. W. Andrews, Lysosomes behave as Ca^{2+}-regulated exocytic vesicles in fibroblasts and epithelial cells. *J. Cell Biol.* **137**, 93–104 (1997).
14. G. Yogalingam, E. J. Bonten, D. van de Vlekkert, H. Hu, S. Moshiach, S. A. Connell, A. d'Azzo, Neuraminidase 1 is a negative regulator of lysosomal exocytosis. *Dev. Cell* **15**, 74–86 (2008).
15. I. Annunziata, A. Patterson, D. Helton, H. Hu, S. Moshiach, E. Gomero, R. Nixon, A. d'Azzo, Lysosomal NEU1 deficiency affects amyloid precursor protein levels and amyloid-β secretion via deregulated lysosomal exocytosis. *Nat. Commun.* **4**, 2734 (2013).
16. E. Machado, S. White-Gilbertson, D. van de Vlekkert, L. Janke, S. Moshiach, Y. Campos, D. Finkelstein, E. Gomero, R. Mosca, X. Qiu, C. L. Morton, I. Annunziata, A. d'Azzo, Regulated lysosomal exocytosis mediates cancer progression. *Sci. Adv.* **1**, e1500603 (2015).
17. X. Wu, K. A. Steigelman, E. Bonten, H. Hu, W. He, T. Ren, J. Zuo, A. d'Azzo, Vacuolization and alterations of lysosomal membrane proteins in cochlear marginal cells contribute to hearing loss in neuraminidase 1-deficient mice. *Biochim. Biophys. Acta* **1802**, 259–268 (2010).
18. E. Zanoteli, D. van de Vlekkert, E. J. Bonten, H. Hu, L. Mann, E. M. Gomero, A. J. Harris, G. Ghersi, A. d'Azzo, Muscle degeneration in neuraminidase 1-deficient mice results from infiltration of the muscle fibers by expanded connective tissue. *Biochim. Biophys. Acta* **1802**, 659–672 (2010).
19. A. D'Azzo, E. Machado, I. Annunziata, Pathogenesis, emerging therapeutic targets and treatment in sialidosis. *Expert Opin. Orphan Drugs* **3**, 491–504 (2015).
20. N. de Geest, E. Bonten, L. Mann, J. de Sousa-Hitzler, C. Hahn, A. d'Azzo, Systemic and neurologic abnormalities distinguish the lysosomal disorders sialidosis and galactosialidosis in mice. *Hum. Mol. Genet.* **11**, 1455–1464 (2002).
21. F. M. Platt, A. d'Azzo, B. L. Davidson, E. F. Neufeld, C. J. Tifft, Lysosomal storage diseases. *Nat. Rev. Dis. Primers.* **4**, 27 (2018).
22. S. J. Mathew, J. M. Hansen, A. J. Merrell, M. M. Murphy, J. A. Lawson, D. A. Hutcheson, M. S. Hansen, M. Angus-Hill, G. Kardon, Connective tissue fibroblasts and Tcf4 regulate myogenesis. *Development* **138**, 371–384 (2011).
23. A. Lorts, J. A. Schwanekamp, T. A. Baudino, E. M. McNally, J. D. Molkentin, Deletion of periostin reduces muscular dystrophy and fibrosis in mice by modulating the transforming growth factor-β pathway. *Proc. Natl. Acad. Sci. U.S.A.* **109**, 10978–10983 (2012).
24. C. N. Pagel, D. K. Wasgewatte Wijesinghe, N. Taghavi Esfandouni, E. J. Mackie, Osteopontin, inflammation and myogenesis: Influencing regeneration, fibrosis and size of skeletal muscle. *J. Cell Commun. Signal.* **8**, 95–103 (2014).
25. G. Sannino, A. Marchetto, T. Kirchner, T. G. P. Grunewald, Epithelial-to-mesenchymal and mesenchymal-to-epithelial transition in mesenchymal tumors: A paradox in sarcomas? *Cancer Res.* **77**, 4556–4561 (2017).
26. H. Kalra, G. P. C. Drummen, S. Mathivanan, Focus on extracellular vesicles: Introducing the next small big thing. *Int. J. Mol. Sci.* **17**, 170 (2016).
27. J. Li, J. Kleeff, H. Kayed, K. Felix, R. Penzel, M. W. Büchler, M. Korc, H. Friess, Glypican-1 antisense transfection modulates TGF-β-dependent signaling in Colo-357 pancreatic cancer cells. *Biochem. Biophys. Res. Commun.* **320**, 1148–1155 (2004).
28. J. P. Webber, L. K. Spary, A. J. Sanders, R. Chowdhury, W. G. Jiang, R. Steadman, J. Wymant, A. T. Jones, H. Kynaston, M. D. Mason, Z. Tabi, A. Clayton, Differentiation of tumour-promoting stromal myofibroblasts by cancer exosomes. *Oncogene* **34**, 290–302 (2015).
29. L. A. Borthwick, T. A. Wynn, A. J. Fisher, Cytokine mediated tissue fibrosis. *Biochim. Biophys. Acta* **1832**, 1049–1060 (2013).

30. D. C. Rockey, P. D. Bell, J. A. Hill, Fibrosis—A common pathway to organ injury and failure. *N. Engl. J. Med.* **372**, 1138–1149 (2015).
31. F. Gattazzo, A. Urciuolo, P. Bonaldo, Extracellular matrix: A dynamic microenvironment for stem cell niche. *Biochim. Biophys. Acta* **1840**, 2506–2519 (2014).
32. T. R. Karhadkar, D. Pilling, N. Cox, R. H. Gomer, Sialidase inhibitors attenuate pulmonary fibrosis in a mouse model. *Sci. Rep.* **7**, 15069 (2017).
33. I. G. Luzina, V. Lockatell, S. W. Hyun, P. Kopach, P. H. Kang, Z. Noor, A. Liu, E. P. Lillehoj, C. Lee, A. Miranda-Ribera, N. W. Todd, S. E. Goldblum, S. P. Atamas, Elevated expression of NEU1 sialidase in idiopathic pulmonary fibrosis provokes pulmonary collagen deposition, lymphocytosis, and fibrosis. *Am. J. Physiol. Lung Cell. Mol. Physiol.* **310**, L940–L954 (2016).
34. T. E. Fingerlin, W. Zhang, I. V. Yang, H. C. Ainsworth, P. H. Russell, R. Z. Blumhagen, M. I. Schwarz, K. K. Brown, M. P. Steele, J. E. Loyd, G. P. Cosgrove, D. A. Lynch, S. Groshong, H. R. Collard, P. J. Wolters, W. Z. Bradford, K. Kossen, S. D. Seiwert, R. M. du Bois, C. K. Garcia, M. S. Devine, G. Gudmundsson, H. J. Isaksson, N. Kaminski, Y. Zhang, K. F. Gibson, L. H. Lancaster, T. M. Maher, P. L. Molyneaux, A. U. Wells, M. F. Moffatt, M. Selman, A. Pardo, D. S. Kim, J. D. Crapo, B. J. Make, E. A. Regan, D. S. Walek, J. J. Daniel, Y. Kamatani, D. Zelenika, E. Murphy, K. Smith, D. McKean, B. S. Pedersen, J. Talbert, J. Powers, C. R. Markin, K. B. Beckman, M. Lathrop, B. Freed, C. D. Langefeld, D. A. Schwartz, Genome-wide imputation study identifies novel HLA locus for pulmonary fibrosis and potential role for auto-immunity in fibrotic idiopathic interstitial pneumonia. *BMC Genet.* **17**, 74 (2016).
35. M. Vizovišek, M. Fonović, B. Turk, Cysteine cathepsins in extracellular matrix remodeling: Extracellular matrix degradation and beyond. *Matrix Biol.* **75–76**, 141–159 (2018).
36. M. A. Nieto, R. Y.-J. Huang, R. A. Jackson, J. P. Thiery, EMT: 2016. *Cell* **166**, 21–45 (2016).
37. J. Farup, L. Madaro, P. L. Puri, U. R. Mikkelsen, Interactions between muscle stem cells, mesenchymal-derived cells and immune cells in muscle homeostasis, regeneration and disease. *Cell Death Dis.* **6**, e1830 (2015).
38. C. F. Ruivo, B. Adem, M. Silva, S. A. Melo, The biology of cancer exosomes: Insights and new perspectives. *Cancer Res.* **77**, 6480–6488 (2017).
39. A. Akhmetshina, K. Palumbo, C. Dees, C. Bergmann, P. Venalis, P. Zerr, A. Horn, T. Kireva, C. Beyer, J. Zwerina, H. Schneider, A. Sadowski, M.-O. Riener, O. A. MacDougald, O. Distler, G. Schett, J. H. W. Distler, Activation of canonical Wnt signalling is required for TGF-β-mediated fibrosis. *Nat. Commun.* **3**, 735 (2012).
40. C. Bergmann, J. H. W. Distler, Canonical Wnt signaling in systemic sclerosis. *Lab. Invest.* **96**, 151–155 (2016).
41. M. Capurro, T. Martin, W. Shi, J. Filmus, Glypican-3 binds to Frizzled and plays a direct role in the stimulation of canonical Wnt signaling. *J. Cell Sci.* **127**, 1565–1575 (2014).
42. Q. Chen, P. Sivakumar, C. Barley, D. M. Peters, R. R. Gomes, M. C. Farach-Carson, S. L. Dallas, Potential role for heparan sulfate proteoglycans in regulation of transforming growth factor-β (TGF-β) by modulating assembly of latent TGF-β-binding protein-1. *J. Biol. Chem.* **282**, 26418–26430 (2007).
43. B. Wang, Z. Tang, H. Gong, L. Zhu, X. Liu, Wnt5a promotes epithelial-to-mesenchymal transition and metastasis in non-small-cell lung cancer. *Biosci. Rep.* **37**, BSR20171092 (2017).
44. D. R. Newman, W. S. Sills, K. Hanrahan, A. Ziegler, K. M. Tidd, E. Cook, P. L. Sannes, Expression of WNT5A in idiopathic pulmonary fibrosis and its control by TGF-β and WNT7B in human lung fibroblasts. *J. Histochem. Cytochem.* **64**, 99–111 (2016).
45. N. Andrejewski, E.-L. Punnonen, G. Guhde, Y. Tanaka, R. Lüllmann-Rauch, D. Hartmann, K. von Figura, P. Saftig, Normal lysosomal morphology and function in LAMP-1-deficient mice. *J. Biol. Chem.* **274**, 12692–12701 (1999).
46. E. Hsu, H. Shi, R. M. Jordan, J. Lyons-Weiler, J. M. Pilewski, C. A. Feghali-Bostwick, Lung tissues in patients with systemic sclerosis have gene expression patterns unique to pulmonary fibrosis and pulmonary hypertension. *Arthritis Rheum.* **63**, 783–794 (2011).

Acknowledgments: We thank I. A. Cusimano for critical reading of the manuscript and insightful suggestions; S. Frase, L. Horner, and R. Wakefield for the EM images; V. Frolich and J. Peters for support with IF imaging; and R. Ashmun for the FACS analyses. We thank P. Saftig for sharing with us the *Lamp1*$^{-/-}$ mouse model. A.d'A. holds the Jewelers for Children Endowed Chair in Genetics and Gene Therapy. **Funding:** This work was supported in part by NIH grants R01GM104981, RO1DK095169, and CA021764, the Assisi Foundation of Memphis, and the American Lebanese Syrian Associated Charities. **Author contributions:** A.d'A. conceived the project and designed and supervised the research. D.v.d.V. and A.d'A. wrote the manuscript. D.v.d.V. designed, performed, and analyzed most of the experiments. J.D. performed and analyzed the exosome proteomic data. Y.C. helped with muscle isolation, processing, and staining, performed some of IF experiments, and gave insightful suggestions on the manuscript. X.-X.N. and C.A.F.-B. designed, performed, and analyzed the human IPF data. E.M. performed some of IF stainings and helped with the culture of NEU1-overexpressing cells and immunoblot experiment. I.A. helped with cell cultures, collection of exosomes, and manuscript editing and revision. H.H. performed paraffin embedding and cutting of tissues and IHC analysis. E.G. maintained the animal colonies and performed the AAV injections. X.Q. purified the anti-NEU1 antibody. A.B. helped with the initial procedure for exosome isolation and critically read the manuscript. **Competing interests:** A.d'A. and I.A. are inventors on a patent related to this work filed by St. Jude Children's Research Hospital (no. US20140193392A1, filed 31 August 2011). All other authors declare that they have no competing interests. **Data and materials availability:** All data needed to evaluate the conclusions in the paper are present in the paper and/or the Supplementary Materials. Additional data related to this paper may be requested from the authors.

Submitted 6 September 2018
Accepted 11 June 2019
Published 17 July 2019
10.1126/sciadv.aav3270

Citation: D. van de Vlekkert, J. Demmers, X.-X. Nguyen, Y. Campos, E. Machado, I. Annunziata, H. Hu, E. Gomero, X. Qiu, A. Bongiovanni, C. A. Feghali-Bostwick, A. d'Azzo, Excessive exosome release is the pathogenic pathway linking a lysosomal deficiency to generalized fibrosis. *Sci. Adv.* **5**, eaav3270 (2019).

Excessive exosome release is the pathogenic pathway linking a lysosomal deficiency to generalized fibrosis

Diantha van de Vlekkert, Jeroen Demmers, Xinh-Xinh Nguyen, Yvan Campos, Eda Machado, Ida Annunziata, Huimin Hu, Elida Gomero, Xiaohui Qiu, Antonella Bongiovanni, Carol A. Feghali-Bostwick and Alessandra d'Azzo

Sci Adv **5** (7), eaav3270.
DOI: 10.1126/sciadv.aav3270